

Oriented Object Detection in Optical Remote Sensing Images using Deep Learning: A Survey

Kun Wang^{a,b,*}, Zi Wang^{a,b,*}, Zhang Li^{a,b,**}, Ang Su^{a,b}, Xichao Teng^{a,b}, Minhao Liu^{a,b} and Qifeng Yu^{a,b}

^aCollege of Aerospace Science and Engineering, National University of Defense Technology, Changsha, 410000, China

^bHunan Provincial Key Laboratory of Image Measurement and Vision Navigation, Changsha, 410000, China

ARTICLE INFO

Keywords:

Oriented object detection
Remote sensing
Deep learning

ABSTRACT

Oriented object detection is one of the most fundamental and challenging tasks in remote sensing, aiming to locate and classify objects with arbitrary orientations. Recent years have witnessed remarkable progress in oriented object detection using deep learning techniques. Given the rapid development of this field, this paper aims to provide a comprehensive survey of recent advances in oriented object detection. To be specific, we first review the technical evolution from horizontal object detection to oriented object detection and summarize the specific challenges, including feature misalignment, spatial misalignment, and periodicity of angle. Subsequently, we further categorize existing methods into detection framework, oriented bounding box (OBB) regression, and feature representations, and discuss how these methods address the above challenges in detail. In addition, we cover several publicly available datasets and performance evaluation protocols. Furthermore, we provide a comprehensive comparison and analysis of state-of-the-art oriented object detection methods. Toward the end of this paper, we discuss several future directions for oriented object detection.

1. Introduction

With the rapid development of remote sensing (RS) technologies, an increasing number of images with various resolutions and different spectra can be easily obtained by optical satellites or unmanned aerial vehicles (UAVs). Naturally, the research community has an urgent demand to investigate a variety of advanced technologies for automatically and efficiently processing and analyzing massive RS images. As a crucial cornerstone of automatic analysis for RS images, object detection aims to recognize objects of predefined categories from given images and to regress a precise localization of each object instance (Liu et al., 2020; Zou et al., 2023). Nowadays, object detection has served as an essential step for a broad range of RS applications, including intelligent monitoring (Zhao et al., 2018; Salvoldi et al., 2022), precision agriculture (Osco et al., 2021), urban planning (Burochin et al., 2014), port management (Zhang et al., 2021a), and military reconnaissance (Liu et al., 2022c).

Objects in RS images typically appear in arbitrary orientations due to the bird-eye view (BEV), making the general (horizontal) object detection methods unsuitable. Different from general object detection that represents object localization via a horizontal bounding box (HBB), oriented object detection (also called rotated object detection) uses an oriented bounding box (OBB) to tightly pack the oriented object, as shown in Figure 1. The OBB can not only provide orientation information but also locate the object precisely.

Consequently, oriented object detection has attracted significant attention, especially in the last five years. While enormous methods exist, a comprehensive survey specifically focused on oriented object detection is still lacking. Given the continued maturity and increasing concerns about this field, this paper attempts to present a thorough analysis of recent efforts and systematically summarize their achievements.

1.1. Comparisons with Related Surveys

In object detection, quite a number of prominent surveys have been published in recent years, as summarized in Table 1. Many notable surveys focus on generic horizontal object detection that aims to detect horizontal objects in natural scenarios (Jiao et al., 2019; Liu et al., 2020; Wu et al., 2020; Zhao et al., 2019; Zou et al., 2023) and cover various aspects, including deep learning based detection frameworks, training strategies, feature representation, evaluation metrics, and typical applications. There also several efforts focused on a specific category, such as face detection (Zafeiriou et al., 2015; Du et al., 2022), text detection (Ye and Doermann, 2015; Yin et al., 2016), and pedestrian detection (Brunetti et al., 2018; Cao et al., 2022). What's more, there are also surveys paying their attention to object detection under specific conditions, including small object detection (Tong et al., 2020; Liu et al., 2021a; Cheng et al., 2023), few-shot object detection (Pannone, 2022; Huang et al., 2023), and weakly-supervised object detection (Zhang et al., 2022a). Although a few surveys analyze and summarize RS object detection, they either lack of in-depth analysis for oriented object detection (Cheng and Han, 2016; Li et al., 2020, 2021; Han et al., 2021b; Wu et al., 2022) or categorize the sub-categories belonging to RS object detection as oriented

*Equal contribution.

**Corresponding author. Email address: lizhang08@nudt.edu.cn.

Table 1

Summary of related object detection surveys in recent years

Survey title	Venue	Descriptions
General object detection		
A Survey of Deep Learning-Based Object Detection (Jiao et al., 2019)	ACCESS	A survey on deep learning frameworks and methods for generic object detection
Deep Learning for Generic Object Detection: A Survey (Liu et al., 2020)	IJCV	A comprehensive survey of the recent progress in generic object detection brought about by deep learning
Recent advances in deep learning for object detection (Wu et al., 2020)	Neucom	A survey focuses on deep learning in generic object detection from detection components, learning strategies, and applications
Object Detection With Deep Learning: A Review (Zhao et al., 2019)	TNNLS	A review on deep learning for generic object detection and other specific subtasks
Object Detection in 20 Years: A Survey (Zou et al., 2023)	PROC	A survey focuses on object detection spanning over 20 years of history
Specific category		
A survey on face detection in the wild: Past, present and future (Zafeiriou et al., 2015)	CVIU	A survey on real-world face detection techniques since 2000
The Elements of End-to-end Deep Face Recognition: A Survey of Recent Advances (Du et al., 2022)	ACM	A survey about each element of end-to-end deep face detection, face alignment, and face representation
Text Detection and Recognition in Imagery: A Survey (Ye and Doermann, 2015)	TPAMI	A survey about methods, sub-problems, and special issues of text detection and recognition
Text Detection, Tracking, and Recognition in Video: A Comprehensive Survey (Yin et al., 2016)	TIP	A survey of text detection, tracking, and recognition methods and systems in the video
Computer vision and deep learning techniques for pedestrian detection and tracking: A survey (Brunetti et al., 2018)	Neucom	A survey on deep learning for pedestrian detection and tracking
From Handcrafted to Deep Features for Pedestrian Detection: A Survey (Cao et al., 2022)	TPAMI	A survey on recent deep features based methods in pedestrian detection
Specific conditions		
Recent advances in small object detection based on deep learning: A review (Tong et al., 2020)	IVC	A survey on small object detection using deep learning
A survey and performance evaluation of deep learning methods for small object detection (Liu et al., 2021a)	ESWA	A survey of challenges, solutions, and deep learning technologies for small object detection
Towards Large-Scale Small Object Detection: Survey and Benchmarks (Cheng et al., 2023)	TPAMI	A survey of small object detection and two large-scale small object detection benchmarks under driving scenario and aerial scene
Few-Shot Object Detection: A Survey (Pannone, 2022)	ACM	A survey on few-shot object detection through data augmentation, transfer learning, distance metric learning, and meta-learning
A Survey of Self-Supervised and Few-Shot Object Detection (Huang et al., 2023)	TPAMI	Categorization, review, and comparison for few-shot and self-supervised object detection methods
Weakly Supervised Object Localization and Detection: A Survey (Zhang et al., 2022a)	TPAMI	A survey on weakly supervised object detection, including classic models, off-the-shelf models, and deep weakly supervised approaches
RS object detection		
A survey on object detection in optical remote sensing images (Cheng and Han, 2016)	ISPRS	A review on traditional object detection methods in RS images
Object detection in optical remote sensing images: A survey and a new benchmark (Li et al., 2020)	ISPRS	A review on deep learning based horizontal object detection in RS, and a large-scale, publicly available benchmark for RS object detection
Remote Sensing Object Detection Meets Deep Learning: A Meta-review of Challenges and Advances (Zhang et al., 2023)	arxiv	A survey on challenges and advances in RS object detection, including multi-scale object detection, rotated object detection, weak object detection, tiny object detection, and object detection with limited supervision
Ship detection and classification from optical remote sensing images: A survey (Li et al., 2021)	CJA	A survey of RS ship detection schemes from 1978 to 2020
Methods for Small, Weak Object Detection in Optical High-Resolution Remote Sensing Images: A survey of advances and challenges (Han et al., 2021b)	MGRS	A survey of challenges and recent advances for RS small, weak object detection
Deep Learning for Unmanned Aerial Vehicle-Based Object Detection and Tracking: A survey (Wu et al., 2022)	MGRS	A survey on deep learning approaches in UAV object detection and tracking from static object detection, video object detection, and multiple object detection

object detection (Zhang et al., 2023). Hence, none is rigorously concentrated on an oriented object detection survey. Given the extremely rapid rate of achievements in this field, a comprehensive survey of previous efforts is crucial for further development. By strictly casting our sight on oriented objects, we thoroughly review hundreds of top journal and conference papers related to oriented object detection in RS images. As a result, a systematic survey of oriented object detection is proposed, which is radically different from previous works. We believe that this survey shall be valuable for researchers to gain a clear understanding of oriented object detection with deep learning.

1.2. Contributions

The major contributions of this work are summarized as follows:

(1) We briefly review the technical evolution from horizontal object detection to oriented object detection and summarize the main challenges, including feature misalignment, spatial misalignment, and PoA.

(2) We systematically summarize recent advancements in oriented object detection and categorize them in three folds according to their motivation: detection frameworks, OBB regression, and feature representations. Meanwhile, we review dozens of RS datasets related to oriented object detection.

(3) We provide a unified comparison of state-of-the-art methods on several typical datasets and an in-depth analysis of the pros and cons of these methods. Furthermore, we identify several promising directions for future research.

The structure of this paper is organized as follows. We first introduce the development from horizontal object detection to oriented object detection and highlight the major challenges in Section 2. Then, we review deep neural networks (DNN) based detection frameworks in Section 3. Furthermore, we discuss the OBB regression and feature representation in Section 4 and Section 5, respectively. In addition, we summarize other common issues encountered in RS scenarios in Section 6. After an overview of commonly used datasets is provided in Section 7, we analyze and compare the state-of-the-art methods in Section 8. Finally, we conclude our work and discuss the future directions of oriented object detection in Section 9.

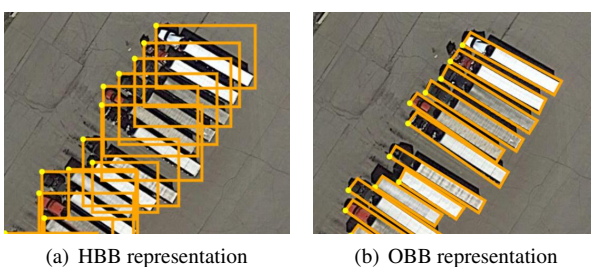


Figure 1: Comparison between OBB and HBB (Xia et al., 2018; Ding et al., 2022). (a) OBB representation of objects. (b) is a failure case of the HBB representation, which brings high overlap compared to (a).

2. From Horizontal Object Detection to Oriented Object Detection

The early object detection methods rely on handcrafted descriptors (Lowe, 2004; Dalal and Triggs, 2005; Fei-Fei and Perona, 2005; Wright et al., 2009) and machine learning approaches (Cortes and Vapnik, 1995; Blaschke, 2010; Leitloff et al., 2010; Blaschke et al., 2014). These methods often show limited performance due to the weak feature representations. Although lag far behind in accuracy, their instructive insights still have a profound impact on modern detectors, *e.g.*, sliding windows (Viola and Jones, 2001, 2004), hard negative mining, and bounding box regression (Felzenszwalb et al., 2008, 2010). The readers interested in early object detection methods are referred to the recent survey (Cheng and Han, 2016) that provides an in-depth analysis of many classical object detection methods in RS.

The world has witnessed impressive progress in computer vision with the advance of deep neural networks (DNN) since 2012 (Hinton and Salakhutdinov, 2006; LeCun et al., 2015; Chen et al., 2018; He et al., 2016; Krizhevsky et al., 2012, 2017). Benefiting from the continuous improvement of computing resources, DNN can learn high-level patterns from large-scale datasets in an end-to-end fashion. The pioneering studies bring a little glimmer to the object detection field, especially in light of the fact that the performance of handcrafted features-based detectors reached a plateau after 2010. Since then, an increasing number of DNN-based detectors have been proposed and have dominated the state-of-the-art due to their powerful feature representation. Early research in the deep learning era was primarily concerned with designing horizontal object detectors (Girshick et al., 2014; Girshick, 2015; Ren et al., 2017; Liu et al., 2016a; Lin et al., 2020; Redmon et al., 2016; Redmon and Farhadi, 2017; Hei and Jia, 2020; Duan et al., 2019; Zhou et al., 2019; Yang et al., 2019b) for natural scene images taken from a horizontal perspective. In contrast, RS images are typically captured from the BEV, leading to objects appearing in arbitrary orientations. Hence, horizontal object detectors may suffer from the following problems in RS images: (1) HBBs are inclined to contain background, causing DNN to hardly capture discriminative features vital to subsequent regression and classification tasks. (2) The intersection-over-union (IoU) between an HBB and the adjacent HBBs can be very large in dense arrangement scenarios, especially for objects with extremely large aspect ratios, as illustrated in Figure 1(a). Thus, the non-maximum suppression (NMS) technique tends to cause missed detection. Given the above predicament of HBB, OBB is considered more appropriate for RS object detection (Figure 1(b)). To advance object detection research in RS images, a vast collection of large-scale datasets well-annotated with OBBs is released, *e.g.*, DOTA (Xia et al., 2018; Ding et al., 2022), which can serve as an impartial platform for comparing various methods. Furthermore, the challenging datasets can advance object detection toward increasingly complex and tough scenarios.

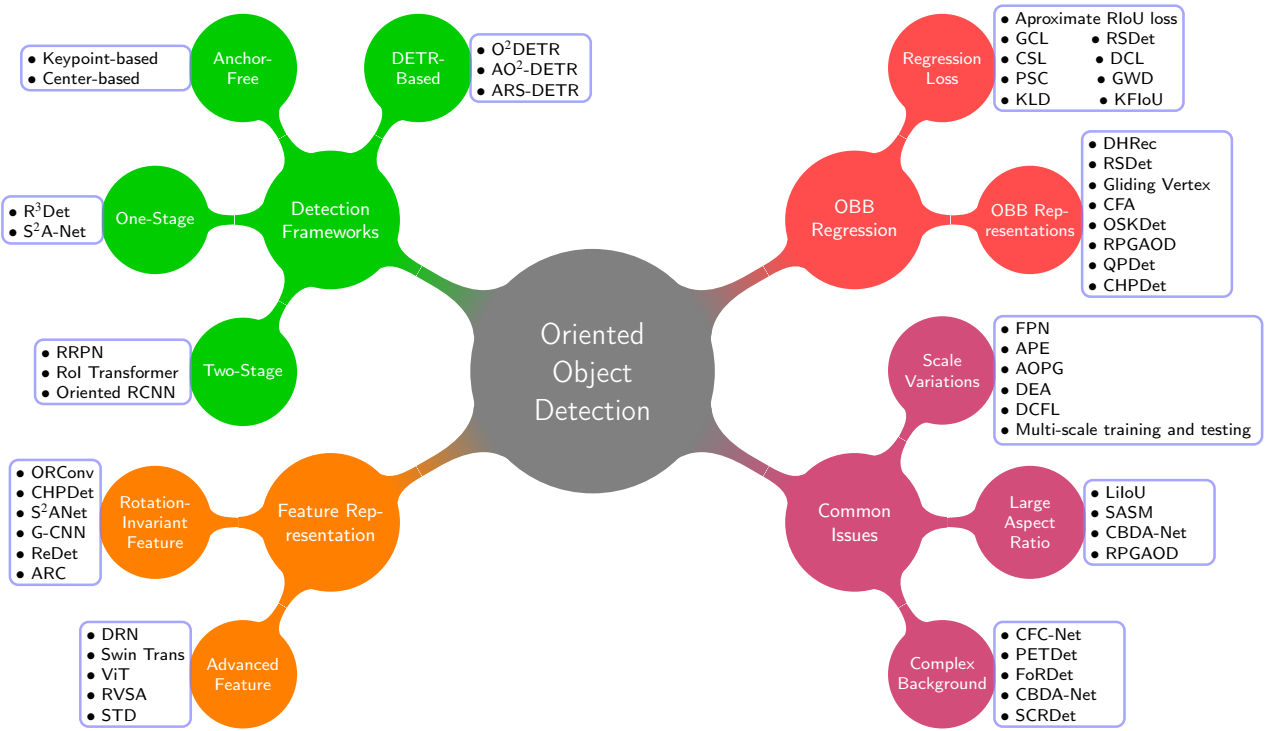


Figure 2: Structured taxonomy of the deep learning based oriented object detection methods in this survey.

With the remarkable development of detection frameworks (Ren et al., 2017; Lin et al., 2020; Redmon et al., 2016; Carion et al., 2020), backbone networks (He et al., 2016; Liu et al., 2021b), and robust feature representation (Liu et al., 2022d; Dosovitskiy et al., 2021), the field of object detection has achieved dramatic breakthroughs. Naturally, an intuitive strategy for designing oriented object detectors is to modify representative horizontal object detectors by incorporating an additional channel that predicts the angle θ (Zhou et al., 2022; Yu and Da, 2023). However, such a straightforward strategy is plagued by several additional challenges, mainly including feature misalignment, spatial misalignment, and periodicity of angle (PoA).

(1) **Feature Misalignment.** The prevailing generic object detectors typically contain a feature extraction network followed by a detection head, where the latter leverages the feature representations generated from the former to make decisions. However, the feature representations are generally extracted via axis-aligned convolutions, thereby exposing non-negligible misalignment with oriented objects. Such a misaligned feature representation is harmful to oriented objects due to the lack of rotational information, making the detector struggle to identify objects and regress precise OBBs.

(2) **Spatial Misalignment.** In addition to feature misalignment, the widely used anchor-based detection methods also struggle with spatial misalignment. Generic anchor-based detectors typically use horizontal anchors as priors thereby having limited overlaps to oriented objects, especially for objects with extremely large aspect ratios. This poses a significant challenge to generic label assignment

strategies (Ren et al., 2017), which assign positive or negative samples depending on the overlaps. Thus, the naïve anchor generation mechanism commonly fails to provide sufficient positive samples during the whole training.

(3) **Periodicity of angle.** Current detectors commonly utilize the regression paradigm to locate objects, which has been proven to be effective and yields dramatic achievement. However, the angle regression will suffer from the PoA, causing the angular boundary discontinuity (Yang et al., 2021c,d; Yang et al., 2022; Qian et al., 2021, 2022). Concretely, a small angle difference may cause a large loss change when the angular value approaches the angular boundary range. Thus, PoA can seriously confuse the network, leading to training instability. For more details please refer to Section A of the Appendix.

To cope with the above dilemmas, various works have been made and achieved notable advancements, which mainly follow two paths. One involves constructing well-designed **detection frameworks** by devising rotated proposal generation networks or refined heads to remedy feature misalignment and spatial misalignment, and the other line of efforts intends to design effective **OBG regression** through developing new loss functions or OBB representation to eliminate PoA. In addition, high-quality **feature representations** are crucial for object detection, hence a great deal of effort is concentrated on network designs for better feature representations. We also cover the solutions for several **common issues** in RS scenarios. In the following, we will systematically analyze and discuss prominent works in oriented object detection from four aspects: Detection Framework (Section 3), OBB Regression (Section 4), Feature Representation

(Section 5), and Common Issues (Section 6). Figure 2 shows the taxonomy of oriented object detection methods in this survey.

3. Detection Frameworks

It is widely accepted that object detection methods generally can be categorized into two groups: two-stage and one-stage detection (Liu et al., 2020; Zou et al., 2023). The former works in a coarse-to-fine paradigm while the latter completes classification and regression in one step thereby enjoying high efficiency but performing poorly on accuracy. Compared with the above two categories using anchor mechanisms, anchor-free methods directly detect objects without preset anchors. In addition, a series of DETR-based methods have merged recently, which view the detection process as a set prediction task, effectively eliminating several hand-craft components, *e.g.*, NMS and anchor mechanism. Considering that each category has pros and cons, we divide the representative oriented object detectors into four categories: two-stage, one-stage, anchor-free, and DETR-based. Next, we will briefly review how each category addresses feature misalignment and spatial misalignment via deliberate framework design.

3.1. Two-Stage

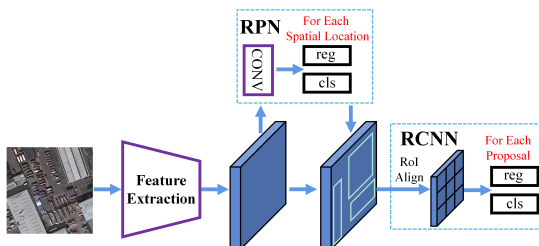


Figure 3: The basic architecture of two-stage detectors.

Among numerous outstanding two-stage detectors (Ren et al., 2017; Lin et al., 2017; Cai and Vasconcelos, 2018; He et al., 2020; Qiao et al., 2021), Faster RCNN (Ren et al., 2017) armed with FPN (Lin et al., 2017) commonly serves as a benchmark due to its high accuracy and efficient design. As illustrated in Figure 3, it consists of the following pipeline: Feature Extraction, Region proposal networks (RPN), and Regions with CNN features (RCNN). In the first stage, a sparse set of high-quality region proposals, that can potentially contain objects, are generated via RPN (Chavali et al., 2016; Hosang et al., 2016). During the second stage, the region features are extracted for each proposal and then used for classification and refined regression using RCNN. Finally, several post-processing operations, such as NMS, are leveraged to output detection results (omitted in Figure 3).

Its oriented version, termed as Rotated Faster RCNN or Faster RCNN OBB, predicts the orientation of each object by adding an extra channel in the regression branch. However, the naïve RPN only generates horizontal region proposals as regions of interest (RoIs), as shown in Figure 4(a). Apart

from the feature misalignment caused by axis-aligned convolutions, another factor that may impair the final performance is the feature misalignment between horizontal RoI (HRoI) and OBB. Thus, the feature misalignment harms the feature representation significantly, making the detectors struggle to identify objects and regress precise OBBs yet inspiring successive innovations.

To cope with the feature misalignment, a variety of efforts are dedicated to generating rotated proposals and then adopting rotated RoI (RRoI) operators to extract spatial-aligned features. RRPN (Ma et al., 2018; Yang et al., 2018; Zhang et al., 2018) are designed with rotated anchors to fit the objects with different orientations. In addition to scales and aspect ratios, different orientation parameters are added to further generate additional rotated anchors, as shown in Figure 4(b). Such a scheme can alleviate the spatial misalignment thereby achieving better performance in terms of recall, but the redundant rotated anchors bring about expensive computation and memory consumption. To reduce the number of rotated anchors, RoI Transformer (Ding et al., 2019) retains the naïve RPN structure and introduces a lightweight learnable module, named RoI Learner. As shown in Figure 4(c), RRPN Learner can convert HRoIs to RRoIs directly. Such a design generates precise RRoIs without enormous rotated anchors, resulting in higher efficiency and accuracy. However, the RRPN Learner involves an additional stage including RoI operator and regression, making the networks complex and inefficient. As a result, Xie et al. (2021) design a simpler structure, named oriented RPN, to generate high-quality RRoIs from horizontal anchors directly (Figure 4(d)). Oriented RPN only contains a 3×3 convolutional layer and two sibling 1×1 convolutional layers. This lightweight module benefits from the proposed midpoint offset representation. For an oriented object, its midpoint offset representation consists of the corresponding external HBB and the offsets of vertexes w.r.t the midpoints of the external HBB. The external HBB can provide bounded constraint for OBB and the offsets can avoid the angle regression. In addition, midpoint offset representation retains the horizontal regression mechanism, making the training more stable than regressing OBBs from horizontal anchors. Benefiting from the design of oriented RPN and midpoint offset representation, Oriented RCNN can achieve competitive accuracy to advanced two-stage detectors and reach approximate efficiency to one-stage detectors.

3.2. One-Stage

Different from two-stage detection frameworks working in a coarse-to-fine paradigm, one-stage detectors complete classification and regression in one step Lin et al. (2020). As illustrated in Figure 5, one-stage detectors first extract multi-level feature maps and then predict the class probabilities and locations for each anchor per spatial location. Since the removal of RPN and RoI operators, one-stage detectors exhibit more severe feature misalignment compared to two-stage ones. Thus, a series of one-stage algorithms are developed to alleviate the dilemma, such as R³Det (Yang et al.,

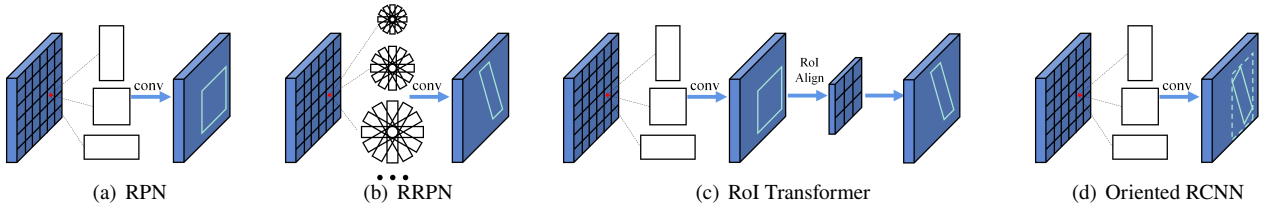


Figure 4: The comparisons of different strategies for proposal generation. (a) RPN only generates horizontal proposals (Ren et al., 2017). (b) RRPN densely places rotated anchors with different scales, ratios, and angles (Ma et al., 2018; Yang et al., 2018; Zhang et al., 2018). (c) ROI Transformer generates rotated proposal from horizontal ROI via RPN, ROI Alignment, and OBB regression (Ding et al., 2019). (d) Oriented RCNN can generate high-quality rotated proposals using a lightweight module (Xie et al., 2021).

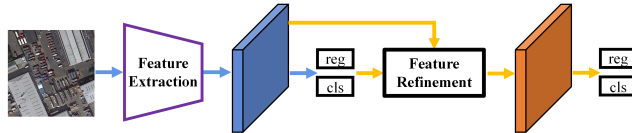


Figure 5: The basic architecture of one-stage detectors. The blue arrows denote the workflow of RetinaNet (Lin et al., 2020), while the yellow arrows denote the workflow of refined stage.

2021b), ADT-Det (Zheng et al., 2021), and S²A-Net (Han et al., 2022).

R³Det (Yang et al., 2021b) adopts a feature refinement module (FRM) to align features. First, R³Det transforms the horizontal anchors into rotated anchors, which can provide more accurate positional and oriented information. Then, FRM employs pixel-wise feature interpolation to integrate features from five locations (*i.e.*, one center and four corners) of the corresponding refined rotated anchors. Similarly, S²A-Net (Han et al., 2022) uses alignment convolution (AlignConv) to align the features. As a variant of deformable convolution (Dai et al., 2017), the offset field of AlignConv is inferred from the guide of rotated anchors. These schemes work in a coarse-to-fine paradigm to align features but are noticeably different from the RRoI operator. The major difference lies in that the FRM or AlignConv follows a full convolution structure and has fewer sampling points than the RRoI operator, making it more efficient.

3.3. Anchor-Free

The above two categories follow the anchor paradigm which suffers from spatial misalignment between horizontal anchor and OBB. To tackle the above issues, a constellation of anchor-free methods is developed to find objects without preset anchors. These methods eliminate anchor-related hyper-parameters, showing potential in the generalization to wide applications (Zhang et al., 2020b). According to the representation of OBB, anchor-free methods can be divided into keypoint-based methods (Guo et al., 2021; Wei et al., 2020) and center-based methods (Guan et al., 2021; He et al., 2021; Lin et al., 2019; Xiao et al., 2020; Yi et al., 2021; Zhang et al., 2022b; Zhou et al., 2020; Zhao et al., 2021).

The keypoint-based methods first locate a set of adaptive or self-constrained key points and then circumscribe the spatial extent of the object, as shown in Figure 6(a). O²-DNet (Wei et al., 2020) first locates the midpoints of four sides of the OBB by regressing the offsets from the center point. Then, two sets of opposite midpoints are connected to form two mutually perpendicular midlines which can be decoded to get the representation of OBB. In addition, a self-supervision loss is designed to constrain the perpendicular relationship between two middle lines and a collinear relationship between the center point and two opposite midpoints. Following the RepPoints (Yang et al., 2019b), CFA (Guo et al., 2021) utilizes the deformable convolution (Dai et al., 2017) to generate a convex hull for each oriented object. The convex hull is represented by a set of irregular sample points bounding the spatial extent of an object, which are determined by the designed Convex Intersection over Union (CIoU) loss. To alleviate feature aliasing between densely packed objects, convex-hull set splitting and feature anti-aliasing strategies are designed to refine the convex-hulls and adaptively optimal feature assignment. Furthermore, to predict the high-quality oriented reppoints, Oriented RepPoints (Li et al., 2022b) further designs an Adaptive Points Assessment and Assignment (APAA) scheme to measure the quality of reppoints. Such a scheme assesses each set of reppoints from four aspects, including classification, localization, orientation alignment, and point-wise correlation. As a result, the high-quality reppoints obtained via APAA enable Oriented RepPoints to achieve state-of-the-art performance among anchor-free methods.

The center-based methods generally generate multiple probabilistic heatmaps and a series of feature maps. As shown in Figure 6(b), the heatmaps provide a set of candidates (peak points) as coarse center points. Meanwhile, the feature maps regress transformation parameters to represent the OBB. Nowadays, most center-based methods are dedicated to designing a variety of OBB representations to address PoA problems (Guan et al., 2021; He et al., 2021; Lin et al., 2019; Xiao et al., 2020; Yi et al., 2021; Zhang et al., 2022b; Zhou et al., 2020; Zhao et al., 2021). However, the center-based methods typically follow the one-stage paradigms and tend to predict coarse locations

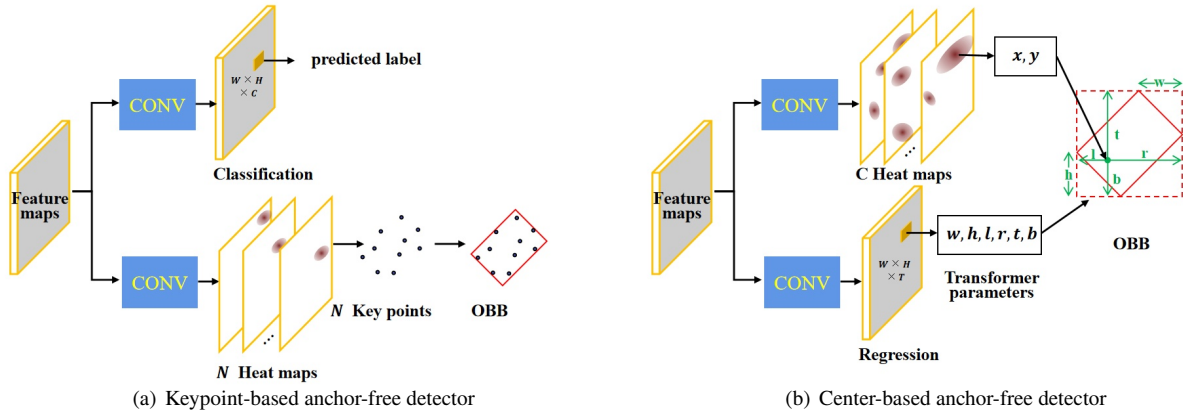


Figure 6: The basic architecture of keypoint-based and center-based anchor-free detectors.

due to feature misalignment, while state-of-the-art methods generally contain one or multiple refined stages to improve performance. Thus, an effective scheme for performance improvement is leveraging anchor-free methods to generate coarse proposals that are then refined to generate high-quality proposals or detection results, *e.g.*, AOPG (Cheng et al., 2022a), DEA (Liang et al., 2022). This could be attributed to the fact that the anchor-free rotated proposal generation scheme can not only generate accurate proposals but also avoid the spatial misalignment caused by horizontal anchors. Nevertheless, there is still a significant performance gap between plain center-based oriented methods and other state-of-the-art methods, necessitating further research.

3.4. DETR-Based

In addition to the above convolution-based methods, DETR-based detectors show great potential and achieve state-of-art performance in the detection community, including DETR (Carion et al., 2020) and its variants (Zhu et al., 2021; Sun et al., 2021; Gao et al., 2021). Based on DETR (Carion et al., 2020), O²DETR (Ma et al., 2021) was proposed to utilize the Transformer for the oriented object detection task. In addition, the depthwise separable convolutions (Sifre and Mallat, 2013; Chollet, 2017; Haase and Amthor, 2020) is introduced to replace the computationally complex self-attention mechanism, making networks more lightweight and speeding up the training. To tackle feature misalignment, Dai et al. (2022) propose AO2-DETR by improving Deformable DETR (Zhu et al., 2021), which design an oriented proposal generation mechanism and an adaptive oriented proposal refinement (OPR) module for aligning the features. Recently, several improved DETR-based detectors have been proposed for generic object detection, *e.g.*, DN-DETR (Li et al., 2022a), DAB-DETR (Liu et al., 2022a), and DINO (Zhang et al., 2022), bringing about dramatic breakthroughs in accuracy and convergence speed. Zeng et al. (2024) propose ARS-DETR that attempts to exploit DINO (Zhang et al., 2022) to oriented object detection tasks. Compared to other advanced oriented object detectors, it achieves greater detection accuracy in the more rigorous

metric (*i.e.*, AP₇₅), but lags behind in the standard metric (*i.e.*, AP₅₀). Worse still, the long training convergence time and heavy computation cost are still open problems.

3.5. Discussion

Feature misalignment and spatial misalignment will seriously impair the performance of oriented object detection. To tackle these issues, an enormous amount of research effort has contributed to modifying the detection frameworks. Existing two-stage detectors typically design efficient and precisely oriented proposal generation modules, which can extract rotated aligned features with RRoI operators. Similarly, one-stage detectors are inclined to add an extra refined stage for feature alignment. Thus, the above two schemes can empower the detectors to mine the rotation-related information, thereby enhancing the semantic representation of oriented objects. Nevertheless, the modules are generally troubled by spatial misalignment. To alleviate this issue, anchor-free detectors discard the anchor mechanism. However, current anchor-free methods generally show limited performance due to feature misalignment. In addition, DETR-based methods provide a new detection paradigm and receive widespread concerns. However, the exploration of DETR-based methods in oriented object detection is not comprehensive enough, requiring further research to accelerate training convergence and reduce computation overheads.

Well-designed detection frameworks are conducive to alleviating feature and spatial misalignment but fail to address the PoA problems. Besides, the extracted features are not equipped with rotation-invariance as the convolution operators are axis-aligned. To cope with the above dilemma, the suitable OBB regression and the powerful feature representation of oriented objects are also widely studied, since they can be seamlessly integrated into various detection frameworks. Next, we will discuss the OBB regression and feature representation.

4. OBB Regression

Oriented object detectors typically locate objects in a regression fashion. The customized regression head predicts the orientation parameters when using the most frequently used θ -based representation. Unfortunately, such a regression paradigm suffers from several limitations, including inconsistency between metric and loss, and angular boundary discontinuity. For more details about the above issues please refer to Section A of the Appendix or corresponding papers (Qian et al., 2021, 2022; Yang et al., 2021c, 2022b; Xu et al., 2021a). To tackle these issues, existing oriented object detection methods usually develop new loss functions or redesign OBB representation. Next, we will briefly introduce these approaches and discuss their pros and cons.

4.1. Regression Loss

(1) **Inconsistency between Metric and Loss.** The inconsistency between metric and loss generally implies that an optimum choice for the regression task may not guarantee a high localization accuracy in terms of IoU. To address this issue, existing generic object detectors generally introduce IoU-induced loss functions, such as GIoU (Rezatofighi et al., 2019) and DIoU (Zheng et al., 2020). However, these IoU-induced losses cannot be incorporated directly into oriented object detection due to the in-differentiable nature of RIoU (Yang et al., 2021c). Thus, several differentiable functions are designed to approximate RIoU loss (Yang et al., 2021b, 2019a, 2022a). Chen et al. (2020) proposed PIoU by introducing a differentiable kernel function, which accumulates the contribution of interior overlapping pixels to approximate the intersection area. Several solutions (Yang et al., 2019a, 2022a, 2021b) integrated RIoU as a loss weight of the regression loss:

$$L_{R\text{IoU}} = \frac{L_{\text{reg}}}{|L_{\text{reg}}|} \cdot |g(R\text{IoU})| \quad (1)$$

L_{reg} denotes the commonly used smooth L1 loss (Ren et al., 2017). $g(\cdot)$ is a loss function related to RIoU, e.g., $-\log(\cdot)$. Such a loss can be divided into two parts, a normalized regression loss $\frac{L_{\text{reg}}}{|L_{\text{reg}}|}$ controlling the direction of gradient propagation, and a scalar $g(R\text{IoU})$ adjusting gradient magnitude. When the RIoU is close to 1, $g(R\text{IoU}) \approx 0$, and L_{reg} is approximately equal to 0, which can effectively alleviate the inconsistency between the metric and regression loss. Apart from designing regression loss to approach RIoU, Ming et al. (2024) analyze the gradient and propose a Gradient Calibration Loss (GCL). GCL build a corrected gradient w.r.t RIoU, angular error, and scale, and then calculate the optimized regression loss through integration. However, angle regression still suffers from the problem of PoA.

(2) **Angular Boundary Discontinuity.** Owing to PoA, the regression loss will sharply increase when the angle approaches its boundary or the aspect ratio closes to 1, seriously confusing the networks and causing training instability. Thus, several methods have been proposed to address these issues, which can be divided into three types:

Modulated rotated loss (Qian et al., 2021, 2022). The modulated Rotated loss adds an extra loss item based on the naïve regression loss to eliminate the angular boundary discontinuity. Specifically, it first transforms the original predicted OBB $b_p = (x_p, y_p, w_p, h_p, \theta_p)$ to another form $b'_p = (x_p, y_p, h_p, w_p, \theta_p - \frac{\pi}{2})^1$, and then take the minimum of their regression loss, i.e., $\min \{L_{\text{reg}}(b_p, b_g), L_{\text{reg}}(b'_p, b_g)\}$, where b_g denotes the corresponding ground-truth OBB. Such a scheme can adaptively choose the appropriate representation of the predicted OBB making the smallest loss value, thereby effectively eliminating the sudden increase in loss when the angle approaches its boundary and ensuring the loss continuous. However, the gap between metric and loss still exists.

Angle coder (Yang and Yan, 2020; Yang et al., 2021a; Yu and Da, 2023). Yang and Yan (2020) proposed a new baseline by transforming the angular regression task into a classification problem. The angle is discretized into a certain number of intervals, and then a discrete angle is predicted by classification. Besides, to increase the error tolerance to adjacent angles and handle the PoA, the circular smooth label (CSL) technique is designed. Although CSL eliminates the boundary discontinuity, its heavy prediction layer harms the efficiency and the square-like problem remains unsolved. To tackle these issues, Yang et al. (2021a) further adopted Densely Coded Labels (DCL) by introducing a lightweight prediction layer, which reduces the code length. Moreover, Angle Distance and Aspect Ratio Sensitive Weighting (ADARSW) were designed to improve the accuracy of square-like objects. However, the hyper-parameters have a significant impact on the performance of CSL and DCL. Even worse, the optimal settings on different datasets are also different thereby requiring laborious tuning. To solve this problem, Yu and Da (2023) designed a differentiable angle coder, named Phase-Shifting Coder (PSC). PSC encodes the angle into a periodic phase to solve the boundary discontinuity problem. Moreover, to further solve the square-like problem, PSCD was proposed by mapping the angle into the phases of different frequencies, which is the advanced dual-frequency version of PSC.

Gaussian distribution based methods (Yang et al., 2021c,d; Yang et al., 2022; Yang et al., 2022b). The Gaussian distribution based methods provide a unified and elegant solution to the problems of boundary discontinuity and the square-like problem. First, the OBB $b = (x, y, w, h, \theta)$ is converted to a 2-D Gaussian distribution $\mathcal{N}(m, \Sigma)$, where $m = (x, y)$ and Σ is a matrix associated with w, h, θ :

$$\Sigma^{\frac{1}{2}} = \begin{bmatrix} \frac{w}{2} \cos^2 \theta + \frac{h}{2} \sin^2 \theta & \frac{w-h}{2} \cos \theta \sin \theta \\ \frac{w-h}{2} \cos \theta \sin \theta & \frac{h}{2} \cos^2 \theta + \frac{w}{2} \sin^2 \theta \end{bmatrix} \quad (2)$$

Then a distance function is used to measure two Gaussian distributions, such as Gaussian Wasserstein Distance

¹It is noteworthy that the modulated rotated loss is customized for OBB representation under the OpenCV definition, which is intractable to the exchangeability of edges and PoA.

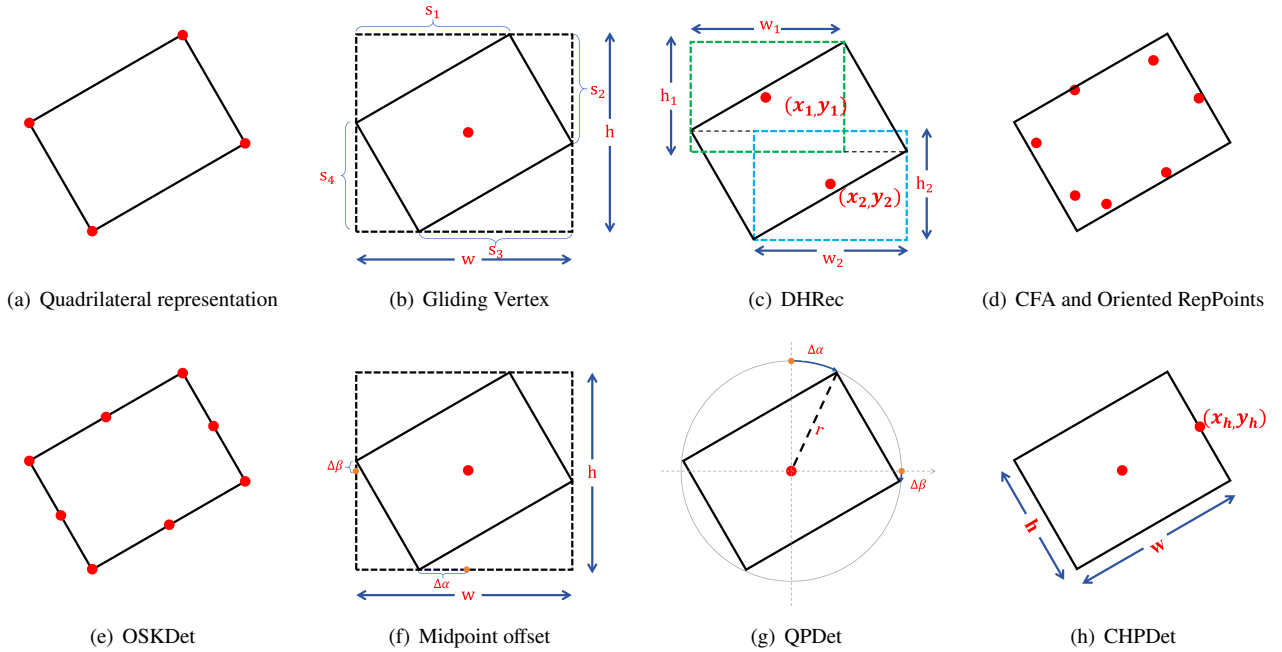


Figure 7: Comparison of different OBB representation methods. The red dots and parameters denote corresponding OBB parameters.

(GWD) (Yang et al., 2021c) or Kullback-Leibler Divergence (KLD) (Yang et al., 2021d). Furthermore, the measure between Gaussian distributions is converted into an approximate IoU loss using a nonlinear transformation to obtain consistency between the metric and the regression loss. The merit of Gaussian distribution is that the angle is encoded by trigonometric function thereby not constrained by PoA. Moreover, the OBB parameters are joint-optimized dynamically so that they can influence each other during training. However, both GWD and KLD only maintain value-level consistency instead of trend-level consistency between RIoU and regression loss. To ameliorate this problem, Yang et al. (2022) design the KFIoU loss based on the Kalman filter to achieve the best trend-level alignment with RIoU, which is differentiable and does not require additional hyperparameters. Based on the mechanism of RIoU, KFIoU calculates the overlapping area between two Gaussian distributions via a Kalman filter. Benefiting from the trend-level alignment strategy, KFIoU achieves better performance than GWD and KLD.

4.2. OBB Representations

To handle the angular boundary discontinuity, the most straightforward approach is to design a novel OBB representation. One scheme exploits new parameters to redefine the OBB, *e.g.*, quadrilateral representation (Xu et al., 2021a), DHRec (Nie and Huang, 2023). The quadrilateral representation adopts coordinates of four vertexes to represent OBB but suffers from the inconsistency of vertex sorting² between predicted OBB and ground truth (Figure 7(a)). RSDet (Qian et al., 2021, 2022) introduces a modulated loss

to avoid the large regression loss caused by vertex sorting, in which the order of the four vertices of the predicted OBB is moved clockwise and counterclockwise by one place respectively. Then, taking the minimum of their regression loss. Xu et al. (2021a) proposed an effective way by gliding the vertex of the horizontal anchor on each corresponding side (Figure 7(b)). Specifically, it regresses four length ratios representing the gliding offset on each corresponding side, which can eliminate the confusion caused by vertex sorting. DHRec (Nie and Huang, 2023) encodes the OBB using double HBBs derived from the sorted horizontal and vertical coordinates (Figure 7(c)). In addition, several anchor-free methods utilize keypoints to denote an OBB, which can provide rich semantic features for oriented objects. Following the RepPoints (Yang et al., 2019b), CFA (Guo et al., 2021) and Oriented RepPoints (Li et al., 2022b) utilize the deformable convolution (Dai et al., 2017) to generate a group of reppoints (Figure 7(d)). Then, a minimum bounding rectangle for each set of predicted reppoints is calculated to obtain detection results. OSKDet (Lu et al., 2022) encodes 8 ordered points (4 vertices and 4 midpoints) to represent an OBB based on the consideration that the object has more obvious features at the vertex and edge areas (Figure 7(e)). Furthermore, an orientation-sensitive heatmap is designed to better fit the shape, allowing the model to learn the orientation and shape of the rotated object implicitly. Although the angular discontinuity has been eliminated, the redesigned OBB representations still have their limitations. Quadrilateral representation is irregular and DHRec adds extra position and oblique factors to ensure the uniqueness of the representations. Meanwhile, the keypoints rely on a

²For more detail please refer to Section B of the Appendix.

complicated post-processing operator to generate a rectangular box.

Therefore, there is another scheme for OBB representation that only uses additional parameters to determine the orientation of objects. A classical way is the midpoint offset representation proposed by Xie et al. (2021), in which the orientation can be inferred via the midpoint offset (Figure 7(f)). However, the midpoint offset representation usually generates a parallelogram and requires a post-processing procedure for regularization. Based on midpoint offset representation, Qiao et al. (2023) analyze the geometric relationship between the OBB and its external HBB to derive the height directly from the width and two offsets, and only use five parameters to generate the high-quality OBB directly from the horizontal anchors. QPDet (Yao et al., 2023) adopt two symmetrical offsets w.r.t the quadrant points to account for rotation and aspect ratio, and a single parameter (radius r) controls the scale (Figure 7(g)). CHPDet (Zhang et al., 2022b) define a head point to indicate the orientation but require proper annotations that specify the direction of the object head in the range of 2π (Figure 7(h)). These strategies of orientation representation can discard angle regression, thus naturally eliminating the angular boundary discontinuity.

4.3. Discussion

As stated above, an enormous amount of research effort is committed to resolving the challenges encountered by OBB regression. Redesigning novel regression loss for mainstream θ -based representation empowers the detectors to solve the inconsistency problem and eliminate the confusion caused by PoA, thereby enhancing the stability of network back-propagation. Especially, Gaussian distribution based methods draw upon the trigonometric encoder and joint-optimization to achieve strong performance. On the other hand, novel OBB representation schemes can avoid angle regression, in which the completely redefined OBB representations commonly rely on complex post-processing or extra constraints, while the orientation representations provide a simple yet efficient way to determine the orientation. Nevertheless, only a handful of novel OBB representation schemes take into account the inconsistency problem.

5. Feature Representation

Robust and discriminative feature representations can significantly improve both localization and classification. As a result, the most recent improvements in detection accuracy have been via research into enhancing feature representation through innovative network architectures. In this section, we review the effort devoted to improving feature representations of oriented objects, *i.e.*, rotation-invariant feature representation, and advanced feature representation.

5.1. Rotation-Invariant Feature Representations

Rotation-invariance is an essential problem when learning visual feature representations for oriented objects (Lowe, 2004; Han et al., 2021a; Yu et al., 2023). The commonly

used approaches, including RRoI operators (Ma et al., 2018; Yang et al., 2018; Ding et al., 2019) and random rotation data augmentation (Han et al., 2021a), are sub-optimal, as they can only extract approximately rotation-invariant features (Lenc and Vedaldi, 2015; Worrall et al., 2017). Recently, the exploration of rotation-sensitive feature extraction networks has brought new insight to the community, which utilize different channels to represent feature information from different orientations, *e.g.*, oriented response convolution (ORConv) (Zhou et al., 2017), group equivariant convolutional neural networks (G-CNN) (Cohen and Welling, 2016; Worrall et al., 2017; Marcos et al., 2017; Weiler and Cesa, 2019; Weiler et al., 2018). Naturally, several works, *e.g.*, RRD (Liao et al., 2018), CHPDet (Zhang et al., 2022b), S²ANet (Han et al., 2022), replace ordinary convolution modules with ORConv to obtain orientation-dependent responses which are then transformed to rotation-invariant features using ORAlign and ORPooling. Besides, ReDet (Han et al., 2021a) incorporates G-CNN into the detector for rotation-equivariant feature generation, whereafter, a rotation-invariant roI align operator is designed to adaptively extract rotation-invariant features from equivariant ones according to the predicted orientations. In contrast to ORConv and G-CNN extracting features via static kernels oriented in a group of fixed orientations, ARC (Pu et al., 2023) rotates the convolution kernels dynamically according to the orientation of the objects, where the orientation is predicted in a data-dependent manner. As a result, ARC can capture the rotation information of objects with different orientations and boost the feature representation under the oriented object detection scenario.

5.2. Advanced Feature Representations

In addition to rotation-invariant networks, advanced feature extraction networks play a crucial role in high-precision detection, *e.g.*, Vision Transformer (Vaswani et al., 2017; Dosovitskiy et al., 2021; Liu et al., 2021b), ConvNext (Liu et al., 2022d). Recently, Vision Transformer has achieved significant success in computer vision (Dosovitskiy et al., 2021; Liu et al., 2021b; Han et al., 2023), which mainly adopts the self-attention mechanism to capture global feature representations. Benefiting from the exceptional feature representation capacity, more and more methods introduce Vision Transformer for object detection and obtain impressive performance. ViT series (Dosovitskiy et al., 2021; Xu et al., 2021b; Zhang et al., 2023b) and Swin Transformer (Liu et al., 2021b) are representative architectures that can directly serve as the backbone networks for object detection, showing more excellent feature representation capability than CNN. An unsupervised pertaining scheme, MAE (He et al., 2022), has made notable progress in developing ViT for object detection. As a result, the powerful Vision Transformer architectures contribute to establishing a solid foundation for delivering outstanding achievements in oriented object detection. Nevertheless, their utilization in oriented object detection is fairly unexplored, *e.g.*, an essential problem is how to extract rotation-related features.

Based on ViT, Wang et al. (2022) design rotated varied-size window attention (RVSA) to adaptively obtain locally oriented windows at different sizes, locations, and angles, enabling detectors to extract more useful oriented information for oriented object detection tasks. Although RVSA outperforms all previous methods, it relies on the self-attention mechanism to create oriented windows, without explicitly leveraging guiding information. STD (Yu et al., 2023) adopts a controlled scheme for manipulating the feature extraction process according to the decoupled OBB parameters, *i.e.*, center position, sizes, and angles. It follows a divide-and-conquer fashion that estimates the position, size, and angle via separate network branches at different stages. Further, the cascaded activation masks created by the decoupled OBB parameters are integrated to gradually enhance features extracted by stacked Transformer blocks. The progressive refinement of feature representation enables STD to reach state-of-the-art performance, achieving 82.24% and 98.55% mAP on DOTA-V1.0 (Xia et al., 2018) and HRSC2016 (Liu et al., 2016b) datasets, respectively. Recently, ConvNeXt (Liu et al., 2022d) gradually modified the standard ResNet according to a series of design decisions of Swin Transformer (Liu et al., 2021b) and demonstrated pure CNNs outperform the vision transformers in terms of accuracy and robustness. Meanwhile, ConvNeXt can maintain the efficiency of standard CNNs, thus becoming the dominant architecture in many applications.

5.3. Discussion

Investigation of feature representation can lead to the improvement of the whole object detection field. ORConv and G-CNN empower the model to mine rotation-invariant features by utilizing different channels to represent feature information from different orientations, while advanced feature extraction networks are dedicated to enhancing the semantic representation via powerful and well-designed architectures. Although the former is conducive to extracting rotation-invariant features in both spatial and channel dimensions, they are built on conventional CNN modules which fall behind the latter. Thus, it's crucial to validate the effectiveness of integrating the rotation-invariant feature extraction networks and advanced ones. We hope further research effort is conducted to explore more powerful rotation-invariant and high-level semantic feature representation for oriented object detection.

6. Common Issues in RS scenarios

In addition to the specific challenges associated with oriented object detection, several common issues still exist regarding RS scenarios, *e.g.*, scale variations, large aspect ratio, and complex background, as shown in Figure 8.

6.1. Scale Variations

As the ground sampling distance (GSD) can range from a few centimeters to hundreds of meters, the RS images taken by different sensors usually have large-scale variations. Additionally, while different kinds of objects may have

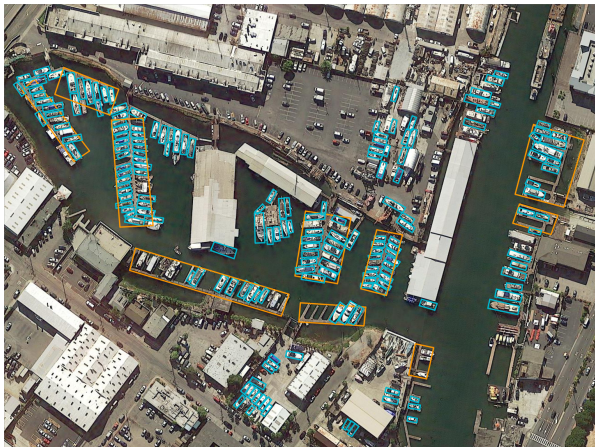
large-scale variations, the instances of the same category also vary in size. Therefore, the inter-class and intra-class scale variations pose additional challenges. Especially, the most critical challenge mainly focuses on small objects due to their insufficient feature information, inaccurate localization, and inadequate positive samples (Cheng et al., 2023). Worse still, things get tougher when it comes to oriented objects due to the extra orientation regression and limited overlaps with anchor boxes.

In recent years, a large number of effective strategies have been made to enhance the robustness and adaptability of detectors for objects with various scales, which can be classified into two categories network-level methods and data-level methods. The former committed to developing novel network structures for multi-scale features extraction, *e.g.*, feature pyramid architectures (Lin et al., 2017) and its variants (Tian et al., 2024), and multi-branch architectures (Li et al., 2019). The latter strives to design data augmentation strategies that are independent of the network architectures and can be generalized to any detectors. Multi-scale training and testing is a useful data augmentation approach that scaling input images at different resolutions (Singh and Davis, 2018; Singh et al., 2018), has been shown to reduce overfitting and improve generalization (Ren et al., 2017; Russakovsky et al., 2015). However, it will inevitably lead to poor time efficiency.

Apart from enhancing the semantic representation or amplifying objects' size, several optimal assignment strategies have emerged to enable adequate sample assignments for small-oriented objects. Since the anchor-free methods can generate more positive samples of small objects that are apt to be ignored in the anchor-based methods, a straightforward scheme is generating samples in an anchor-free manner rather than an anchor-based manner and then refining them to obtain high-quality detection results, *e.g.*, APE (Zhu et al., 2020), AOPG (Cheng et al., 2022a). Furthermore, Liang et al. (2022) propose a dynamic enhancement anchor network that combines the advantages of anchor-free and anchor-based methods and uses an interactive sample screening procedure to generate higher-quality training samples. In contrast to using static priors (*e.g.*, anchor boxes or points) with fixed stride, Xu et al. (2023) design a dynamic prior with a coarse-to-fine assigner. Concretely, it first uses deformable convolution (Dai et al., 2017) to adaptively adjust the prior location and then leverages the coarse prior matching and finer posterior constraint to dynamically assign samples. Such a strategy can adaptively assign positive or negative samples according to the objects' shape and posterior information, boosting the performance of mainstream detectors on small objects.

6.2. Large Aspect Ratio

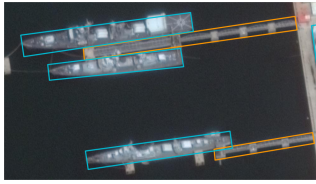
RS images commonly contain some categories with an extremely large aspect ratio, such as bridges, ships, and harbors. The RIoU between these categories with anchors is heavily sensitive to the orientation error, thereby causing



(a) Complex backgrounds



(b) Scale Variations



(c) Large aspect ratio

Figure 8: Illustration of issues in RS scenarios (Xia et al., 2018; Ding et al., 2022). (a)~(c) Examples of scale Variations, large aspect ratio, and complex backgrounds, respectively.

two typical challenges, *i.e.*, spatial misalignment and inaccurate localization. Accordingly, a series of well-designed assignment strategies and regression loss are proposed to remedy corresponding issues. Zhu et al. (2020) propose length-independent IoU (LiIoU) that intercepts part of the object box along its long side based on the length of the anchor and then calculates the IoU between the intercepted object box and anchor. The LiIoU contributes to assigning more positive samples for long objects than naïve IoU, thus improving the recall rate. Following ATSS (Zhang et al., 2020b), SASM (Hou et al., 2022) design a monotonic decreasing function of aspect ratio as a weight for the IoU threshold that controls the sample assignment, enabling the long objects to be assigned a low IoU threshold. Additionally, several methods (Liu et al., 2022b; Qiao et al., 2023) construct the weighted orientation loss depending on aspect ratio, which can decrease the effect of aspect ratio on orientation regression.

6.3. Complex Backgrounds

Due to the wide visual field and complex earth's surface, RS images typically contain a variety of complex backgrounds, causing significant interference in detection. Objects are frequently surrounded by different backgrounds, requiring detectors to possess sufficient discrimination. Besides, there may be backgrounds containing textures and shapes similar to objects, causing a large number of false alarms. To this end, a series of efforts have been made to suppress background noise and emphasize the valuable

areas of the objects. CFC-Net (Ming et al., 2022) and PETDet (Li et al., 2024) both combine channel attention and spatial attention modules to learn the semantic correlation between foreground and background. Such a strategy follows a self-attention mechanism, thus lacking the guidance of the foreground regions. To enhance the discrimination of foreground, FoRDet (Zhang et al., 2022) proposes a foreground relation module for foreground-contextual representations under the supervision of the designed foreground map. Similarly, CBDA-Net (Liu et al., 2022b) builds two parallel spatial attention streams to capture center and boundary attention features, which could assist detectors in improving object localization accuracy. Besides, SCRDet (Yang et al., 2019a) adopts the pixel attention network to generate a saliency map that can separate foreground from background, and use Squeeze-and-Excitation (SE) blocks (Hu et al., 2020) as the channel attention network to enhance the saliency map further. Following this paradigm, SCRDet++ (Yang et al., 2022a) proposes an instance-level denoising (InLD) module that weakens the feature response of the background region while decouples the features of different categories into their corresponding channels.

6.4. Discussion

Scale variations, large aspect ratio, and complex background are crucial issues in RS object detection tasks, which evolve more severely when it comes to oriented object detection tasks. As stated above, a number of works have been proposed to tackle these issues from various perspectives, *e.g.*, data augmentation, assignment strategies, re-weighted orientation loss, and attention mechanism. Unfortunately, exploration into solutions for these issues is far from mature and so further research may be beneficial. For instance, there is still a significant performance gap in detecting small/long and normal objects even for state-of-the-art detectors. On the other hand, the general split-and-detect scheme is inefficient during inference due to too many empty patches that only contain background. Several prior works have provided preliminary consideration on these points, *e.g.*, super-resolution-based object detection (Shermeyer and Van Etten, 2019; Liu et al., 2023; Zhang et al., 2023a), focus-and-detect schemes (Duan et al., 2021; Koyun et al., 2022).

7. Datasets and Performance Evaluation

7.1. Datasets

As a data-driven technology, deep learning is inseparable from various datasets (Everingham et al., 2010; Russakovsky et al., 2015; Lin et al., 2014; Kuznetsova et al., 2020). Throughout the history of object detection, datasets have played an indispensable role not only in training models but also as an impartial platform for evaluating and verifying various methods (Liu et al., 2020). With the rapid

Table 2

Comparison of public RS image datasets.

Dataset	Category	Quantity	Instance	GSD	Resolution
SZTAKI-INRIA (Benedek et al., 2012)	1	9	665	-	600 × 500 ~ 1400 × 800
3K vehicle (Liu and Mattyus, 2015)	1	20	14235	0.13m	5516 × 3744
VEDAI (Razakarivony and Jurie, 2016)	9	1210	3640	0.125m	1024 × 1024
UCAS-AOD (Zhu et al., 2015)	2	2420	14596	-	1280 × 659
HRSC2016 (Liu et al., 2016b)	25	1070	2976	0.4~2m	300 × 300 ~ 1500 × 900
DOTA-V1.0 (Xia et al., 2018)	15	2806	188282	0.1~4.5m	800 × 800 ~ 20000 × 20000
DOTA-V1.5	16	2806	403318	0.1~4.5m	800 × 800 ~ 20000 × 20000
DOTA-V2.0 (Ding et al., 2022)	18	11268	1793658	0.1~4.5m	800 × 800 ~ 29200 × 27620
FGSD (Chen et al., 2020)	43	5634	2612	0.12~1.93m	930 × 930
ShipRSImageNet (Zhang et al., 2021b)	50	3435	17573	0.12~6m	930 × 930 ~ 1400 × 1000
DIOR-R (Cheng et al., 2022a)	20	23463	192518	0.5~30m	800 × 800

development of earth observation technologies, an enormous amount of high-quality RS images can be easily collected to build large-scale datasets. Recently, several research groups have released dozens of high-quality RS image datasets, each of which dramatically boosts the development of RS object detection. Datasets annotated only with HBBs are not covered here, including DIOR (Li et al., 2020), LEVIR (Zou and Shi, 2018), NWPU VHR-10 (Cheng et al., 2014), RSOD (Xiao et al., 2015; Long et al., 2017), xView (Lam et al., 2018), and HRRSD (Zhang et al., 2019). In this subsection, we only focus on introducing RS datasets annotated with OBBs, including SZTAKI-INRIA (Benedek et al., 2012), 3K vehicle (Liu and Mattyus, 2015), UCAS-AOD (Zhu et al., 2015), VEDAI (Razakarivony and Jurie, 2016), HRSC2016 (Liu et al., 2016b), DOTA (Xia et al., 2018; Ding et al., 2022), ShipRSImageNet (Zhang et al., 2021b), and DIOR-R (Cheng et al., 2022a)]. Table 2 statistics the parameters of the above RS datasets for intuitive comparison, and only the most typical among them are described in detail due to the space restriction. For more details please refer to Section C of Appendix.

DOTA (Xia et al., 2018; Ding et al., 2022) contains large quantities of objects with a considerable variety of orientations, scales, and appearances. The images are selected from different sensors and platforms, including Google Earth, GF-2 Satellite, and UAVs. There are three versions of this dataset. The number of images and instances in three versions of DOTA are summarized in Table 3. DOTA-V1.0 (Xia et al., 2018) and DOTA-V1.5 share the same images, which are split into training, validation, and test subsets. As an extension of DOTA-V1.0, DOTA-V1.5 annotates extremely small instances whose sizes are equal to or less than 10 pixels. Compared with the previous versions, DOTA-V2.0 (Ding et al., 2022) contains more images collected from Google Earth, GF-2 Satellites, and aerial platforms. In addition, a large number of images are taken under an oblique view and a lower foreground ratio to approach the real-world application scenes. The number of instances has increased to about 1.8 million. Moreover, it contains two test subsets, namely test-dev and test-challenge. The latter comprises a greater number of object instances

Table 3

Comparison of the three versions of DOTA. The number of images and instances of each split subset is counted.

		V1.0	V1.5	V2.0
Images	Training	1,411		1,830
	Validation	458		593
	Test/Test-dev	937		2,792
	Test-challenge	-		6,053
	Total	2,806		11,268
Instances	Training	98,990	210,631	268,627
	Validation	28,853	69,565	81,048
	Test/Test-dev	60,439	121,893	353,346
	Test-challenge	-	-	1,090,637
	Total	188,282	403,318	1,793,658

(around 1.1 million) and more complicated scenes, making the task more challenging.

DIOR-R (Cheng et al., 2022a) is a large-scale dataset that contains 192,518 instances, covering 20 common categories with notable inter-class similarity and intra-class discrepancies. There are 23,463 images chosen carefully from more than 80 countries thereby possessing richer variations in viewpoint, illumination, background, appearance, occlusion, etc. In addition, the GSD ranges from 0.5m to 30m, causing a large range of size variations. Thus, the rich diversity among instances, images, and scales makes this dataset valuable for real-world tasks yet brings about challenges.

Ship Datasets. Recently, a series of ship datasets have drawn wide attention owing to the potential value of ship detection in fishing, maritime security, and national defense. **HRSC2016** (Liu et al., 2016b) is one of the most widely used datasets for evaluating algorithms of oriented object detection. It covers more than 25 categories of ships with large varieties of scales, orientations, appearances, shapes, and backgrounds (e.g., sea, port). **FGSD** (Chen et al., 2020) is a new fine-grained ship detection dataset expanded based on HRSC2016. The instances are classified

into 43 categories which are further divided into 4 high-level categories, including submarine, aircraft carrier, civil ship, and warship. Except for ships, a new category named dock is also annotated in this dataset for future research. **ShipRSImageNet** (Zhang et al., 2021b) is the largest RS dataset for ship detection. It contains 3,435 images collected from xView (Lam et al., 2018), HRSC2016 (Liu et al., 2016b), FGSD (Chen et al., 2020), Airbus Ship Detection Challenge, and Chinese satellites. A total number of 17,573 ships are divided into 50 categories. There are diverse spatial resolutions, scales, aspect ratios, backgrounds, and orientations in this dataset.

7.2. Evaluation Protocol

Accuracy and efficiency are both the most crucial criteria in evaluating the performance of oriented object detectors. The evaluation protocol for OBB is slightly different from that for HBB as IoU is replaced with RIoU. Efficiency evaluation uses frame per second (FPS), defined as the number of image frames processed by a detector per second, while accuracy evaluation takes into account both precision and recall. The most universally agreed metric for accuracy evaluation is average precision (AP).

For the object detection task, the detector outputs M predicted results $\{(b_j, c_j, s_j)\}_{j=1}^M$, wherein each item contains an OBB b_j , and a category label c_j with corresponding confidence score s_j . Then, the predicted results are assigned to GT objects $\{(b_k^*, c_k^*)\}_{k=1}^N$ based on RIoU and category, where b_k^* , c_k^* and the superscript * denotes the OBB, category label, and GT respectively. A predicted result (b_j, c_j, s_j) which is assigned a GT object (b_k^*, c_k^*) is judged to be a true positive (TP) if the following criteria are met:

(1) The predicted label c_j is in accordance with the label c_k^* of GT object.

(2) The RIoU between the predicted OBB b_j and the GT OBB b_k^* , denoted by RIoU (b, b^*) , is not smaller than the predefined RIoU threshold T_{RIoU} . Otherwise, it is regarded as a false positive (FP).

Once the number of TP and FP has been obtained, precision and recall can be calculated. Precision is the proportion of correctly predicted instances among the total predicted results, while recall is the proportion of all positive instances predicted by the detector among the total GT objects. The formulas are defined as follows:

$$Prec(T_s) = \frac{N_{TP}}{N_{TP} + N_{FP}} \quad (3)$$

$$Rec(T_s) = \frac{N_{TP}}{N_{TP} + N_{FN}} = \frac{N_{TP}}{N} \quad (4)$$

where N_{TP} , N_{FP} , and N_{FN} denote the number of TP, FP, and false negative (FN), respectively, which are determined by score threshold T_s and T_{RIoU} . Note that the precision and the recall are functions of the confidence threshold T_s with a fixed T_{RIoU} .

However, neither precision nor recall can evaluate the accuracy of a detector independently, while AP can combine

both precision and recall. For each category, by varying T_s from 1.0 to 0.0 gradually, the recall increases as N_{TP} increases, and a list of pairs $(Prec, Rec)$ can be obtained. This allows precision to be considered as a discrete function of recall, *i.e.*, the precision-recall curve (PRC), denoted by $P(R)$. The AP value is obtained by computing the average value of precision $P(R)$ over the interval from $R = 0.0$ to $R = 1.0$:

$$AP = \frac{1}{N} \sum_{n=0}^{Rec(0)} \max_{R \geq \frac{n}{N}} P(R) \quad (5)$$

Ultimately, to evaluate the overall accuracy of all categories, the mean AP (mAP) averaged over all categories is adopted as the final metric of evaluation.

8. State-of-the-Art Methods

As a comprehensive survey on oriented object detection, this paper introduces recent advances and provides a structural taxonomy based on detection frameworks, OBB representations, and Other strategies in Sections 3, 4, and 5, respectively. In this section, we select several publicly available detectors to compare them in a unified manner. Specifically, we take DOTA-V1.0 dataset since it contains almost all the typical challenges of this task, including arbitrary orientations, large-scale variations, and large aspect ratio. We report the performance of the state-of-the-art detectors in terms of mAP in Table 4. The top three scores in each category are marked in **red**, **blue**, and **bold**, respectively. According to the performance comparison and previous discussion, we concentrate on the key elements that evolved in oriented object detection, including detection frameworks, OBB regression, feature representations, and data augmentation.

(1) Detection frameworks.

Two-stage detectors achieve the best performance in terms of mAP since they can extract accurate region-based features more suited for classification and regression tasks. The typical two-stage oriented object detection methods commonly designed a rotated proposal generation scheme to obtain more accurate proposals, such as RoI Transformer (Ding et al., 2019) and Oriented RCNN (Xie et al., 2021). Similarly, the majority of one-stage detectors introduce a refined stage to align features, including R³Det (Yang et al., 2021b), S²ANet (Han et al., 2022), CFA (Guo et al., 2021), and Oriented RepPoints (Li et al., 2022b). Benefiting from the additional refined stage and the advanced loss functions, one-stage detectors can also reach approximate accuracy to two-stage detectors.

(2) OBB regression.

Advanced loss functions are conducive to alleviating the problems caused by orientation parameters and achieving better regression in one-stage detectors, including GWD (Yang et al., 2021c), KLD (Yang et al., 2021d), and KFIoU (Yang et al., 2022). As can be seen in the results of multi-scale training and testing, when taking ResNet-152 as the backbone R³Det-GWD, R³Det-KLD, and R³Det-KFIoU outperform

R^3 Det (Yang et al., 2021b) by 3.76%, 4.16%, and 4.56% in terms of mAP, respectively. In particular, for objects with a large aspect ratio, such as bridge (BR) and harbor (HB), as well as objects with a large scale, such as ground track field (GTF) and Roundabout (RA), R^3 Det with advanced loss functions can achieve approximate 10% mAP improvement. The reason may be that Gaussian distribution based methods can jointly optimize the OBB parameters. Nevertheless, there is a huge gap between different OBB representations, *e.g.*, the midpoint offset representation enable oriented RCNN to outperform all other OBB representation methods.

(3) Feature representations.

As one of the most important components in oriented object detection, backbone networks play a critical role in learning high-level semantic feature representation. The most widely used backbone networks include ResNet (He et al., 2016; Xie et al., 2017) series and Transformer architectures (Dosovitskiy et al., 2021; Xu et al., 2021b; Zhang et al., 2023b; Liu et al., 2021b). Although Transformer-based methods have dominated the majority of computer vision tasks, they slightly outperform CNN-based counterparts in oriented object detection. Specifically, Oriented RCNN-RVSA (Wang et al., 2022) and Oriented RCNN-STD (Yu et al., 2023), as the top-performing detectors based on Transformer, only surpasses Oriented RCNN (Xie et al., 2021) by 0.37% and 1.37% in terms of mAP, respectively. In addition, compared to CNNs, Transformers suffer from longer training convergence time and expensive computing costs.

(4) Data augmentation.

The multiscale training and testing (MS) generally first resize the original images to three scales (*i.e.*, $\{0.5, 1.0, 1.5\}$), which are then cropped to patches of $1,024 \times 1,024$ with a stride of 524. In contrast, the single scale training and testing (SS) only crops the original images to patches of $1,024 \times 1,024$ with a stride of 824. As seen in Table 4, detectors with MS achieve an average approximate 3% improvement in terms of mAP. For objects with a large scale, such as ground track field (GTF) and soccer ball field (SBF), and objects with small scale and weak features, such as helicopter (HC), MS promotes detectors by 6 ~ 8% in terms of mAP. Extensive experiments have proven that MS is a useful strategy to alleviate scale variations. However, MS suffers from extremely long times for training and inference, which are about 10 times that of SS.

9. Conclusions and Future Directions

Oriented object detection in RS images is an important and challenging task in the field of RS and has been actively investigated. As summarized in this survey, a variety of methods have been developed rapidly in recent years, showing remarkable progress. In this survey, we first review the evolution from horizontal to oriented object detection and summarize the typical challenges. Following that, we provide a structural taxonomy for detection frameworks and highlight milestone detectors. We also present a detailed elaboration of OBB regression and feature representations.

Furthermore, we discuss the common issues in RS scenarios and corresponding methods. Finally, we summarize commonly used datasets and compare the excellent methods emerging in recent years.

Apart from the above-stated research mentioned in this survey, there is still much work to be done in this field. Next, our goal is to share some insights on future directions, highlighting what is worth exploring to further this field.

Domain Adaptation. The training process of conventional deep learning based models is generally based on the *i.i.d.* assumption that the training and testing samples have identical and independent distribution (Schölkopf et al., 2007). Generally, as data-driven techniques, conventional deep learning based methods rely heavily on the diversity of training data to adapt to different scenarios. However, collecting and annotating enough RS images of all possible domains for model training is expensive, time-consuming, and even prohibitively impossible, especially in the military field (Wang and Deng, 2018; Wang et al., 2021a). In real-world RS applications, oriented object detectors may need to process various images collected at different times (day or night, summer or winter), in different sensors (*e.g.*, SAR, optical, LIDAR, infrared), or under different conditions (weather, illuminance, camera pose, image quality), resulting in the domain distribution gaps between training images and testing images and degrading the performance at test time. To this end, it is desirable to investigate useful and efficient domain adaptation theories and techniques that can guide model design and enhance the generalization capability of the detectors. Recently, a large amount of valuable and instructive methods for domain adaptation have achieved many inspiring results on visual tasks, including discrepancy-based methods (Yosinski et al., 2014), adversarial-based methods (Goodfellow et al., 2014; Tzeng et al., 2017), and reconstruction-based methods (Ghifary et al., 2015, 2016).

Multimodal Information Fusion. Multimodal data has become easy to access in both military and civil fields with the rapid development of a variety of RS technologies, such as Global Positioning System (GPS), Inertial Measurement Unit (IMU), UAV, satellite, and various sensors. In recent years, the most popular multimodal information fusion methods are based on attention mechanisms (Nam et al., 2017) and bilinear pooling (Ben-younes et al., 2017), which have provided remarkable improvements for applications related to image captioning (Vinyals et al., 2015), text-to-image generation (Zhu et al., 2019), and visual question answering (Wang et al., 2018). Although multimodal information fusion methods are attracting growing attention (Zhang et al., 2020a), there are still several challenging problems in the fields of RS and oriented object detection that are far from being solved. The first problem is how to integrate various multimodal RS information, including the poses of sensors, multispectral data, and point clouds, to improve detection performance, since these data are drastically different from each other naturally. Furthermore, multimodal information fusion technologies are important in extending

Table 4

Comparisons of state-of-the-art methods on DOTA-V1.0.

Method	Backbone	PL ¹	BD	BR	GTF	SV	LV	SH	TC	BC	ST	SBF	RA	HA	SP	HC	mAP
Single-scale																	
R ³ Det (Yang et al., 2021b)	R101	88.76	83.09	50.91	67.27	76.23	80.39	86.72	90.78	84.68	83.24	61.98	61.35	66.91	70.63	53.94	73.79
S ² ANet (Han et al., 2022)	R101	88.70	81.41	54.28	69.75	78.04	80.54	88.04	90.69	84.75	86.22	65.03	65.81	76.16	73.37	58.86	76.11
One- CFA* (Guo et al., 2021)	R-152	89.08	83.20	54.37	66.87	81.23	80.96	87.17	90.21	84.32	86.09	52.34	69.94	75.52	80.76	67.96	76.67
stage R ³ Det-KLD (Yang et al., 2021d)	R50	88.90	84.17	55.80	69.35	78.72	84.08	87.00	89.75	84.32	85.73	64.74	61.80	76.62	78.49	70.89	77.36
R ³ Det-GWD (Yang et al., 2021c)	R-152	88.74	82.63	54.88	70.11	78.87	84.59	87.37	89.81	84.79	86.47	66.58	64.11	75.31	78.43	70.87	77.57
Oriented RepPoints* (Li et al., 2022b)	Swin-T	89.11	82.32	56.71	74.95	80.70	83.73	87.67	90.81	87.11	85.85	63.60	68.60	75.95	73.54	63.76	77.63
S ² ANet-GCL (Ming et al., 2024)	Swin-T	89.02	84.72	57.21	74.72	80.68	84.11	88.68	90.87	87.36	87.20	65.60	70.08	76.91	78.55	65.35	78.73
ROI Trans. (Ding et al., 2019)	R101	88.64	78.52	43.44	75.92	68.81	73.68	83.59	90.74	77.27	81.46	58.39	53.54	62.83	58.93	47.67	69.56
SCRDet (Yang et al., 2019a)	R101	89.98	80.65	52.09	68.36	68.36	60.32	72.41	90.85	87.94	86.86	65.02	66.68	66.25	68.24	65.21	72.61
Gliding Vertex (Xu et al., 2021a)	R50	89.64	85.00	52.26	77.34	73.01	73.14	86.82	90.74	79.02	86.81	59.55	70.91	72.94	70.86	57.32	75.02
AOPG* (Cheng et al., 2022a)	R101	89.14	82.74	51.87	69.28	77.65	82.42	88.08	90.89	86.26	85.13	60.60	66.30	74.05	67.76	58.77	75.39
Two- DODet (Cheng et al., 2022b)	R101	89.61	83.10	51.43	72.02	79.16	81.99	87.71	90.89	86.53	84.56	62.21	65.38	71.98	70.79	61.93	75.89
stage SCRDet++ (Yang et al., 2022a)	R101	89.77	83.90	56.30	73.98	72.60	75.63	82.82	90.76	87.89	86.14	65.24	63.17	76.05	68.06	70.24	76.20
ReDet (Han et al., 2021a)	ReR50	88.79	82.64	53.97	74.00	78.13	84.06	88.04	90.89	87.78	85.75	61.76	60.39	75.96	68.07	63.59	76.25
QPDet (Yao et al., 2023)	R50	89.55	83.66	54.06	73.93	78.93	83.08	88.29	90.89	86.60	82.03	65.55	74.16	70.09	58.16	76.25	
Oriented RCNN (Xie et al., 2021)	R101	88.86	83.48	55.27	76.92	74.27	82.10	87.52	90.90	85.56	85.33	65.51	66.82	74.36	70.15	57.28	76.28
RPGAOD (Qiao et al., 2023)	R50	89.34	83.53	54.39	76.59	78.09	81.44	87.64	90.83	85.89	85.33	65.44	64.96	73.73	70.31	59.50	76.47
Oriented RCNN-ARC (Pu et al., 2023)	ARC-R101	89.39	83.58	57.51	75.94	78.75	83.58	88.08	90.90	85.93	85.38	64.03	68.65	75.59	72.03	65.68	77.70
AO2-DETR (Dai et al., 2022)	R50	89.27	84.97	56.67	74.89	78.87	82.73	87.35	90.50	84.68	85.41	61.97	69.96	74.68	72.39	71.62	77.73
Oriented RCN-RVSA(Wang et al., 2022)	ViTAE	89.38	84.26	59.39	73.19	79.99	85.36	88.08	90.87	88.50	86.53	58.93	72.24	77.31	79.59	71.24	78.99
Multi-scale																	
R ³ Det (Yang et al., 2021b)	R-152	89.80	83.77	48.11	66.77	78.76	83.27	87.84	90.82	85.38	85.51	65.67	62.68	67.53	78.56	72.62	76.47
R ³ Det-DCL (Yang et al., 2021a)	R-152	89.26	83.60	53.54	72.76	79.04	82.56	87.31	90.67	86.59	86.98	67.49	66.88	73.29	70.56	69.99	77.37
One- S ² ANet (Han et al., 2022)	R50	88.89	83.60	57.74	81.95	79.94	83.19	89.11	90.78	84.87	87.81	70.30	68.25	78.30	77.01	69.58	79.42
stage R ³ Det-GWD (Yang et al., 2021c)	R-152	89.66	84.99	59.26	82.19	78.97	84.83	87.70	90.21	86.54	86.85	73.47	67.77	76.92	79.22	74.92	80.23
R ³ Det-KLD (Yang et al., 2021d)	R-152	89.92	85.13	59.19	81.33	78.82	84.38	87.50	89.80	87.33	87.00	72.57	71.35	77.12	79.34	78.68	80.63
R ³ Det-KF1IoU (Yang et al., 2022)	R-152	88.89	85.14	60.05	81.13	81.78	85.71	88.27	90.87	87.12	87.91	69.77	73.70	79.25	81.31	74.56	81.03
S ² ANet-GCL (Ming et al., 2024)	Swin-T	89.40	85.19	60.39	79.88	81.37	85.80	88.99	90.85	85.73	88.02	70.38	73.52	83.56	82.49	75.63	81.41
SCRDet++ (Yang et al., 2022a)	R101	90.05	84.39	55.44	73.99	77.54	71.11	86.05	90.67	87.32	87.08	69.62	68.90	73.74	71.29	65.08	76.81
AO2-DETR (Dai et al., 2022)	R50	89.95	84.52	56.90	74.83	80.86	83.47	88.47	90.87	86.12	88.55	63.21	65.09	79.09	82.88	73.46	79.22
ReDet (Han et al., 2021a)	ReR50	88.81	82.48	60.83	80.82	78.34	86.06	88.31	90.87	88.77	87.03	68.65	66.90	79.26	79.71	74.67	80.10
Two-stage ReDet-DEA (Liang et al., 2022)	ReR50	89.92	83.84	59.65	79.88	80.11	87.96	88.17	90.31	88.93	88.46	68.93	65.94	78.04	79.69	75.75	80.37
DODet (Cheng et al., 2022b)	R50	89.96	85.52	58.01	81.22	78.71	85.46	88.59	90.89	87.12	87.80	70.50	71.54	82.06	77.43	74.47	80.62
AOPG* (Cheng et al., 2022a)	R50	89.88	85.57	60.90	81.51	78.70	85.29	88.85	90.89	87.60	87.65	71.66	68.69	82.31	77.32	73.10	80.66
Oriented RCNN (Xie et al., 2021)	R50	89.84	85.43	61.09	79.82	79.71	85.35	88.82	90.88	86.68	87.73	72.21	70.80	82.42	78.18	74.11	80.87
Rol Trans.-KF1IoU (Yang et al., 2022)	Swin-T	89.44	84.41	62.22	82.51	80.10	86.07	88.68	90.90	87.32	88.38	72.80	71.95	78.96	74.95	75.27	80.93
QPDet (Yao et al., 2023)	R50	90.14	85.31	60.98	79.92	80.21	85.04	88.80	90.87	86.45	88.04	70.88	71.72	82.99	80.55	73.19	81.00
RPGAOD (Qiao et al., 2023)	R50	89.93	85.00	60.16	81.58	79.63	84.94	88.71	90.90	86.24	87.65	72.94	72.61	81.24	79.78	76.76	81.20
Oriented RCNN-RVSA(Wang et al., 2022)	ViTAE	88.97	85.76	61.46	81.27	79.98	85.31	88.30	90.84	85.06	87.50	66.77	73.11	84.75	81.88	77.58	81.24
Oriented RCNN-STD (Yu et al., 2023)	HiViT-B	89.15	85.03	60.79	82.06	80.90	85.76	88.45	90.83	87.71	87.29	73.99	71.25	85.18	82.17	82.95	82.24

¹ PL: plane. BD: baseball diamond. BR: bridge. GTF: ground track field. SV: small vehicle. LV: large vehicle. SH: ship. TC: tennis court. BC: baseball court. ST: storage tank. SBF: soccer ball field. RA: roundabout. HA: harbor. SP: swimming pool. HC: helicopter.

2 The results of these methods are the best-reported results from corresponding papers. * indicates anchor-free methods.

oriented object detection to other RS applications, including instance segmentation (Chen et al., 2019) and object tracking (Wen et al., 2021). Finally, transferring well-trained detectors to other modalities is also a challenging task.

Lightweight Methods. The demand for deploying a real-time object detector on resource-constrained mobile devices has grown rapidly. Therefore, achieving a better trade-off between accuracy and efficiency for detectors is of significant importance. To this end, various lightweight architectures have been proposed to reduce computational complexity and spatial complexity without harming accuracy. Several works try to redesign lightweight network architectures based on hand-crafted technologies (Jiang et al., 2022) or Neural Architecture Search (Xiong et al., 2021). Another branch of work presents various compression schemes for compressing networks, including parameter pruning (Hanson and Pratt, 1988; Han et al., 2015), quantization (Song et al., 2016), and knowledge distillation (Hinton et al., 2015). Excellent lightweight generic object detection methods (Xiong et al., 2021; Jiang et al., 2022; Mehta and Rastegari, 2021) depend on the ingenious designs of lightweight feature extraction networks and the efficient information transmission mechanism. Such practices provide an enormous reference value for oriented object detection. In addition, different lightweight methods

may be synergistic and complementary to each other. Thus, reasonable design and combination can achieve outstanding performance. The development of lightweight methods is conducive to the promotion and real-world application of oriented object detection in the RS field, which drives the requirement for further research.

References

Ben-younes, H., Cadene, R., Cord, M., Thome, N., 2017. Mutan: Multimodal tucker fusion for visual question answering, in: IEEE International Conference on Computer Vision, pp. 2631–2639. doi:10.1109/ICCV.2017.285.

Benedek, C., Descombes, X., Zerubia, J., 2012. Building development monitoring in multitemporal remotely sensed image pairs with stochastic birth-death dynamics. IEEE Transactions on Pattern Analysis and Machine Intelligence. 34, 33–50. doi:10.1109/TPAMI.2011.94.

Blaschke, T., 2010. Object based image analysis for remote sensing. ISPRS Journal of Photogrammetry and Remote Sensing. 65, 2–16. doi:10.1016/j.isprsjprs.2009.06.004.

Blaschke, T., Hay, G.J., Kelly, M., Lang, S., Hofmann, P., Addink, E., Queiroz Feitosa, R., van der Meer, F., van der Werff, H., van Coillie, F., Tiede, D., 2014. Geographic object-based image analysis – towards a new paradigm. ISPRS Journal of Photogrammetry and Remote Sensing. 87, 180–191. doi:10.1016/j.isprsjprs.2013.09.014.

Brunetti, A., Buongiorno, D., Trotta, G.F., Bevilacqua, V., 2018. Computer vision and deep learning techniques for pedestrian detection and tracking: A survey. Neurocomputing. 300, 17–33. doi:10.1016/j.neucom.2018.01.092.

Burochin, J.P., Vallet, B., Brédif, M., Mallet, C., Brosset, T., Paparoditis, N., 2014. Detecting blind building façades from highly overlapping wide angle aerial imagery. *ISPRS Journal of Photogrammetry and Remote Sensing*. 96, 193–209. doi:10.1016/j.isprsjprs.2014.07.011.

Cai, Z., Vasconcelos, N., 2018. Cascade r-cnn: Delving into high quality object detection, in: *IEEE/CVF Conference on Computer Vision and Pattern Recognition*, pp. 6154–6162. doi:10.1109/CVPR.2018.00644.

Cao, J., Pang, Y., Xie, J., Khan, F.S., Shao, L., 2022. From handcrafted to deep features for pedestrian detection: A survey. *IEEE Transactions on Pattern Analysis and Machine Intelligence*. 44, 4913–4934. doi:10.1109/TPAMI.2021.3076733.

Carion, N., Massa, F., Synnaeve, G., Usunier, N., Kirillov, A., Zagoruyko, S., 2020. End-to-end object detection with transformers, in: *European Conference on Computer Vision*, pp. 213–229. doi:10.1007/978-3-030-58452-8_13.

Chavali, N., Agrawal, H., Mahendru, A., Batra, D., 2016. Object-proposal evaluation protocol is ‘gameable’, in: *IEEE/CVF Conference on Computer Vision and Pattern Recognition*, pp. 835–844. doi:10.1109/CVPR.2016.97.

Chen, K., Pang, J., Wang, J., Xiong, Y., Li, X., Sun, S., Feng, W., Liu, Z., Shi, J., Ouyang, W., Loy, C.C., Lin, D., 2019. Hybrid task cascade for instance segmentation, in: *IEEE/CVF Conference on Computer Vision and Pattern Recognition*, pp. 4969–4978. doi:10.1109/CVPR.2019.00511.

Chen, K., Wu, M., Liu, J., Zhang, C., 2020. FGSD: A Dataset for Fine-Grained Ship Detection in High Resolution Satellite Images. *arXiv e-prints*, arXiv:2003.06832.

Chen, L.C., Papandreou, G., Kokkinos, I., Murphy, K., Yuille, A.L., 2018. DeepLab: Semantic image segmentation with deep convolutional nets, atrous convolution, and fully connected crfs. *IEEE Transactions on Pattern Analysis and Machine Intelligence*. 40, 834–848. doi:10.1109/TPAMI.2017.2699184.

Chen, Z., Chen, K., Lin, W., See, J., Yu, H., Ke, Y., Yang, C., 2020. Piou loss: Towards accurate oriented object detection in complex environments, in: *European Conference on Computer Vision*, pp. 195–211. doi:10.1007/978-3-030-58558-7_12.

Cheng, G., Han, J., 2016. A survey on object detection in optical remote sensing images. *ISPRS Journal of Photogrammetry and Remote Sensing*. 117, 11–28. doi:10.1016/j.isprsjprs.2016.03.014.

Cheng, G., Han, J., Zhou, P., Guo, L., 2014. Multi-class geospatial object detection and geographic image classification based on collection of part detectors. *ISPRS Journal of Photogrammetry and Remote Sensing*. 98, 119–132. doi:10.1016/j.isprsjprs.2014.10.002.

Cheng, G., Wang, J., Li, K., Xie, X., Lang, C., Yao, Y., Han, J., 2022a. Anchor-free oriented proposal generator for object detection. *IEEE Transactions on Geoscience and Remote Sensing*. 60, 1–11. doi:10.1109/TGRS.2022.3183022.

Cheng, G., Yao, Y., Li, S., Li, K., Xie, X., Wang, J., Yao, X., Han, J., 2022b. Dual-aligned oriented detector. *IEEE Transactions on Geoscience and Remote Sensing*. 60, 1–11. doi:10.1109/TGRS.2022.3149780.

Cheng, G., Yuan, X., Yao, X., Yan, K., Zeng, Q., Xie, X., Han, J., 2023. Towards large-scale small object detection: Survey and benchmarks. *IEEE Transactions on Pattern Analysis and Machine Intelligence*. , 1–20. doi:10.1109/TPAMI.2023.3290594.

Chollet, F., 2017. Xception: Deep learning with depthwise separable convolutions, in: *IEEE/CVF Conference on Computer Vision and Pattern Recognition*, pp. 1800–1807. doi:10.1109/CVPR.2017.195.

Cohen, T.S., Welling, M., 2016. Group equivariant convolutional networks, in: *International Conference on Machine Learning*, pp. 2990–2999. URL: <https://proceedings.mlr.press/v48/cohen16.html>.

Cortes, C., Vapnik, V., 1995. Support-vector networks. *Machine Learning*. 20, 273–297. doi:10.1023/A:1022627411411.

Cui, Y., Jia, M., Lin, T.Y., Song, Y., Belongie, S., 2019. Class-balanced loss based on effective number of samples, in: *IEEE/CVF Conference on Computer Vision and Pattern Recognition*, pp. 9260–9269. doi:10.1109/CVPR.2019.00949.

Dai, J., Qi, H., Xiong, Y., Li, Y., Zhang, G., Hu, H., Wei, Y., 2017. Deformable convolutional networks, in: *IEEE International Conference on Computer Vision*, pp. 764–773. doi:10.1109/ICCV.2017.89.

Dai, L., Liu, H., Tang, H., Wu, Z., Song, P., 2022. Ao2-detr: Arbitrary-oriented object detection transformer. *IEEE Transactions on Circuits and Systems for Video Technology*. , 1–1. doi:10.1109/TCSVT.2022.3222906.

Dalal, N., Triggs, B., 2005. Histograms of oriented gradients for human detection, in: *IEEE Computer Society Conference on Computer Vision and Pattern Recognition*, pp. 886–893. doi:10.1109/CVPR.2005.177.

Ding, J., Xue, N., Long, Y., Xia, G.S., Lu, Q., 2019. Learning roi transformer for oriented object detection in aerial images, in: *IEEE/CVF Conference on Computer Vision and Pattern Recognition*, pp. 2844–2853. doi:10.1109/CVPR.2019.00296.

Ding, J., Xue, N., Xia, G.S., Bai, X., Yang, W., Yang, M.Y., Belongie, S., Luo, J., Datcu, M., Pelillo, M., Zhang, L., 2022. Object detection in aerial images: A large-scale benchmark and challenges. *IEEE Transactions on Pattern Analysis and Machine Intelligence*. 44, 7778–7796. doi:10.1109/TPAMI.2021.3117983.

Dosovitskiy, A., Beyer, L., Kolesnikov, A., Weissenborn, D., Zhai, X., Unterthiner, T., Dehghani, M., Minderer, M., Heigold, G., Gelly, S., 2021. An image is worth 16x16 words: Transformers for image recognition at scale, in: *International Conference on Learning Representations*.

Du, H., Shi, H., Zeng, D., Zhang, X.P., Mei, T., 2022. The elements of end-to-end deep face recognition: A survey of recent advances. *ACM Computing Surveys*. 54, 1–42.

Duan, C., Wei, Z., Zhang, C., Qu, S., Wang, H., 2021. Coarse-grained density map guided object detection in aerial images, in: *IEEE/CVF International Conference on Computer Vision Workshops*, pp. 2789–2798. doi:10.1109/ICCVW54120.2021.00313.

Duan, K., Bai, S., Xie, L., Qi, H., Huang, Q., Tian, Q., 2019. Centernet: Keypoint triplets for object detection, in: *IEEE/CVF International Conference on Computer Vision*, pp. 6568–6577. doi:10.1109/ICCV.2019.00667.

Everingham, M., Gool, L.V., Williams, C.K.I., Winn, J., Zisserman, A., 2010. The pascal visual object classes (voc) challenge. *International Journal of Computer Vision*. 88, 303–338. doi:10.1007/s11263-009-0275-4.

Fei-Fei, L., Perona, P., 2005. A bayesian hierarchical model for learning natural scene categories, in: *IEEE Computer Society Conference on Computer Vision and Pattern Recognition*, pp. 524–531. doi:10.1109/CVPR.2005.16.

Felzenszwalb, P., McAllester, D., Ramanan, D., 2008. A discriminatively trained, multiscale, deformable part model, in: *IEEE/CVF Conference on Computer Vision and Pattern Recognition*, pp. 1–8. doi:10.1109/CVPR.2008.4587597.

Felzenszwalb, P.F., Girshick, R.B., McAllester, D., 2010. Cascade object detection with deformable part models, in: *IEEE/CVF Conference on Computer Vision and Pattern Recognition*, pp. 2241–2248. doi:10.1109/CVPR.2010.5539906.

Gao, P., Zheng, M., Wang, X., Dai, J., Li, H., 2021. Fast convergence of detr with spatially modulated co-attention, in: *IEEE/CVF International Conference on Computer Vision*, pp. 3601–3610. doi:10.1109/ICCV48922.2021.00360.

Ghifary, M., Kleijn, W.B., Zhang, M., Balduzzi, D., 2015. Domain generalization for object recognition with multi-task autoencoders, in: *IEEE International Conference on Computer Vision*, pp. 2551–2559. doi:10.1109/ICCV.2015.293.

Ghifary, M., Kleijn, W.B., Zhang, M., Balduzzi, D., Li, W., 2016. Deep reconstruction-classification networks for unsupervised domain adaptation, in: *European Conference on Computer Vision*, pp. 597–613. doi:10.1007/978-3-319-46493-0_36.

Girshick, R., 2015. Fast r-cnn, in: *IEEE International Conference on Computer Vision*, pp. 1440–1448. doi:10.1109/ICCV.2015.169.

Girshick, R., Donahue, J., Darrell, T., Malik, J., 2014. Rich feature hierarchies for accurate object detection and semantic segmentation, in: *IEEE/CVF Conference on Computer Vision and Pattern Recognition*, pp. 580–587. doi:10.1109/CVPR.2014.81.

Goodfellow, I.J., Pouget-Abadie, J., Mirza, M., Xu, B., Warde-Farley, D., Ozair, S., Courville, A., Bengio, Y., 2014. Generative adversarial nets, in: *International Conference on Neural Information Processing Systems - Volume 2*, p. 2672–2680. doi:10.5555/2969033.2969125.

Guan, Q., Qu, Z., Zeng, M., Shen, J., Du, J., 2021. Cgp box: An effective direction representation strategy for oriented object detection in remote sensing images. *International Journal of Remote Sensing*. 42, 6666–6687. doi:10.1080/01431161.2021.1941389.

Guo, Z., Liu, C., Zhang, X., Jiao, J., Ji, X., Ye, Q., 2021. Beyond bounding-box: Convex-hull feature adaptation for oriented and densely packed object detection, in: *IEEE/CVF Conference on Computer Vision and Pattern Recognition (CVPR)*, pp. 8788–8797. doi:10.1109/CVPR46437.2021.00868.

Gupta, A., Dollár, P., Girshick, R., 2019. Lvis: A dataset for large vocabulary instance segmentation, in: *IEEE/CVF Conference on Computer Vision and Pattern Recognition*, pp. 5351–5359. doi:10.1109/CVPR.2019.00550.

Haase, D., Amthor, M., 2020. Rethinking depthwise separable convolutions: How intra-kernel correlations lead to improved mobilenets, in: *IEEE/CVF Conference on Computer Vision and Pattern Recognition*, pp. 14588–14597. doi:10.1109/CVPR42600.2020.01461.

Han, J., Ding, J., Li, J., Xia, G.S., 2022. Align deep features for oriented object detection. *IEEE Transactions on Geoscience and Remote Sensing*. 60, 1–11. doi:10.1109/TGRS.2021.3062048.

Han, J., Ding, J., Xue, N., Xia, G.S., 2021a. Redet: A rotation-equivariant detector for aerial object detection, in: *IEEE/CVF Conference on Computer Vision and Pattern Recognition*, pp. 2785–2794. doi:10.1109/CVPR46437.2021.00281.

Han, K., Wang, Y., Chen, H., Chen, X., Guo, J., Liu, Z., Tang, Y., Xiao, A., Xu, C., Xu, Y., Yang, Z., Zhang, Y., Tao, D., 2023. A survey on vision transformer. *IEEE Transactions on Pattern Analysis and Machine Intelligence* 45, 87–110. doi:10.1109/TPAMI.2022.3152247.

Han, S., Pool, J., Tran, J., Dally, W.J., 2015. Learning both weights and connections for efficient neural networks, in: *International Conference on Neural Information Processing Systems - Volume 1*, p. 1135–1143. doi:10.5555/2969239.2969366.

Han, W., Chen, J., Wang, L., Feng, R., Li, F., Wu, L., Tian, T., Yan, J., 2021b. Methods for small, weak object detection in optical high-resolution remote sensing images: A survey of advances and challenges. *IEEE Geoscience and Remote Sensing Magazine*. 9, 8–34. doi:10.1109/MGRS.2020.3041450.

Hanson, S.J., Pratt, L.Y., 1988. Comparing biases for minimal network construction with back-propagation, in: *International Conference on Neural Information Processing Systems*, p. 177–185. doi:10.5555/2969735.2969756.

He, K., Chen, X., Xie, S., Li, Y., Dollár, P., Girshick, R., 2022. Masked autoencoders are scalable vision learners, in: *IEEE/CVF Conference on Computer Vision and Pattern Recognition*, pp. 15979–15988. doi:10.1109/CVPR52688.2022.01553.

He, K., Gkioxari, G., Dollár, P., Girshick, R., 2020. Mask r-cnn. *IEEE Transactions on Pattern Analysis and Machine Intelligence*. 42, 386–397. doi:10.1109/TPAMI.2018.2844175.

He, K., Zhang, X., Ren, S., Sun, J., 2016. Deep residual learning for image recognition, in: *IEEE/CVF Conference on Computer Vision and Pattern Recognition*, pp. 770–778. doi:10.1109/CVPR.2016.90.

He, X., Ma, S., He, L., Ru, L., Wang, C., 2021. Learning rotated inscribed ellipse for oriented object detection in remote sensing images. *Remote Sensing*. 13. doi:10.3390/rs13183622.

Hei, L., Jia, D., 2020. Cornernet: Detecting objects as paired keypoints. *International Journal of Computer Vision*. 128, 642–656. doi:10.1007/s11263-019-01204-1.

Hinton, G., Salakhutdinov, R., 2006. Reducing the dimensionality of data with neural networks. *Science*. 313, 504–507. doi:10.1126/science.1127647.

Hinton, G., Vinyals, O., Dean, J., 2015. Distilling the Knowledge in a Neural Network. *arXiv e-prints*. , arXiv:1503.02531.

Hosang, J., Benenson, R., Dollár, P., Schiele, B., 2016. What makes for effective detection proposals? *IEEE Transactions on Pattern Analysis and Machine Intelligence*. 38, 814–830. doi:10.1109/TPAMI.2015.2465908.

Hou, L., Lu, K., Xue, J., Li, Y., 2022. Shape-adaptive selection and measurement for oriented object detection, in: *AAAI Conference on Artificial Intelligence*, pp. 923–932. doi:10.1609/aaai.v36i1.19975.

Hu, J., Shen, L., Albanie, S., Sun, G., Wu, E., 2020. Squeeze-and-excitation networks. *IEEE Transactions on Pattern Analysis and Machine Intelligence*. 42, 2011–2023. doi:10.1109/TPAMI.2019.2913372.

Huang, G., Laradji, I., Vázquez, D., Lacoste-Julien, S., Rodríguez, P., 2023. A survey of self-supervised and few-shot object detection. *IEEE Transactions on Pattern Analysis and Machine Intelligence*. 45, 4071–4089. doi:10.1109/TPAMI.2022.3199617.

Jiang, Y., Tan, Z., Wang, J., Sun, X., Lin, M., Li, H., 2022. GiraffeDet: A Heavy-Neck Paradigm for Object Detection. *arXiv e-prints*. , arXiv:2202.04256.

Jiao, L., Zhang, F., Liu, F., Yang, S., Li, L., Feng, Z., Qu, R., 2019. A survey of deep learning-based object detection. *IEEE Access*. 7, 128837–128868. doi:10.1109/ACCESS.2019.2939201.

Koyun, O.C., Keser, R.K., İbrahim Batuhan Akkaya, Töreyin, B.U., 2022. Focus-and-detect: A small object detection framework for aerial images. *Signal Processing: Image Communication*. 104, 116675. doi:10.1016/j.image.2022.116675.

Krizhevsky, A., Sutskever, I., Hinton, G.E., 2012. Imagenet classification with deep convolutional neural networks, in: *International Conference on Neural Information Processing Systems*, Curran Associates Inc., Red Hook, NY, USA. pp. 1097–1105.

Krizhevsky, A., Sutskever, I., Hinton, G.E., 2017. Imagenet classification with deep convolutional neural networks. *Communications of the ACM*. 60, 84–90. doi:10.1145/3065386.

Kuznetsova, A., Rom, H., Alldrin, N., Uijlings, J., Krasin, I., Pont-Tuset, J., Kamali, S., Popov, S., Malloci, M., Kolesnikov, A., Duerig, T., Ferrari, V., 2020. The open images dataset v4: Unified image classification, object detection, and visual relationship detection at scale. *International Journal of Computer Vision*. , 1956–1981doi:10.1007/S11263-020-01316-Z.

Lam, D., Kuzma, R., McGee, K., Dooley, S., Laielli, M., Klaric, M., Bulatov, Y., McCord, B., 2018. xView: Objects in Context in Overhead Imagery. *arXiv e-prints*. , arXiv:1802.07856.

LeCun, Y., Bengio, Y., Hinton, G., 2015. Deep learning. *Nature*. 521, 436–444. doi:10.1038/nature14539.

Leitloff, J., Hinz, S., Stilla, U., 2010. Vehicle detection in very high resolution satellite images of city areas. *IEEE Transactions on Geoscience and Remote Sensing*. 48, 2795–2806. doi:10.1109/TGRS.2010.2043109.

Lenc, K., Vedaldi, A., 2015. Understanding image representations by measuring their equivariance and equivalence, in: *IEEE/CVF Conference on Computer Vision and Pattern Recognition*, pp. 991–999. doi:10.1109/CVPR.2015.7298701.

Li, B., Xie, X., Wei, X., Tang, W., 2021. Ship detection and classification from optical remote sensing images: A survey. *Chinese Journal of Aeronautics*. 34, 145–163. doi:10.1016/j.cja.2020.09.022.

Li, F., Zhang, H., Liu, S., Guo, J., Ni, L.M., Zhang, L., 2022a. Dn-detr: Accelerate detr training by introducing query denoising, in: *IEEE/CVF Conference on Computer Vision and Pattern Recognition*, pp. 13609–13617. doi:10.1109/CVPR52688.2022.01325.

Li, K., Wan, G., Cheng, G., Meng, L., Han, J., 2020. Object detection in optical remote sensing images: A survey and a new benchmark. *ISPRS Journal of Photogrammetry and Remote Sensing*. 159, 296–307. doi:10.1016/j.isprsjprs.2019.11.023.

Li, W., Chen, Y., Hu, K., Zhu, J., 2022b. Oriented repoints for aerial object detection, in: *IEEE/CVF Conference on Computer Vision and Pattern Recognition*, pp. 1819–1828. doi:10.1109/CVPR52688.2022.00187.

Li, W., Zhao, D., Yuan, B., Gao, Y., Shi, Z., 2024. Petdet: Proposal enhancement for two-stage fine-grained object detection. *IEEE Transactions on Geoscience and Remote Sensing*. 62, 1–14. doi:10.1109/TGRS.2023.3343453.

Li, Y., Chen, Y., Wang, N., Zhang, Z.X., 2019. Scale-aware trident networks for object detection, in: *IEEE/CVF International Conference on Computer Vision*, pp. 6053–6062. doi:10.1109/ICCV.2019.00615.

Liang, D., Geng, Q., Wei, Z., Vorontsov, D.A., Kim, E.L., Wei, M., Zhou, H., 2022. Anchor retouching via model interaction for robust object detection in aerial images. *IEEE Transactions on Geoscience and Remote Sensing*. 60, 1–13. doi:10.1109/TGRS.2021.3136350.

Liao, M., Zhu, Z., Shi, B., Xia, G.s., Bai, X., 2018. Rotation-sensitive regression for oriented scene text detection, in: IEEE/CVF Conference on Computer Vision and Pattern Recognition, pp. 5909–5918. doi:10.1109/CVPR.2018.00619.

Lin, T.Y., Dollár, P., Girshick, R., He, K., Hariharan, B., Belongie, S., 2017. Feature pyramid networks for object detection, in: IEEE/CVF Conference on Computer Vision and Pattern Recognition (CVPR), pp. 936–944. doi:10.1109/CVPR.2017.106.

Lin, T.Y., Goyal, P., Girshick, R., He, K., Dollár, P., 2020. Focal loss for dense object detection. *IEEE Transactions on Pattern Analysis and Machine Intelligence*. 42, 318–327. doi:10.1109/TPAMI.2018.2858826.

Lin, T.Y., Maire, M., Belongie, S., Hays, J., Perona, P., Ramanan, D., Dollár, P., Zitnick, C.L., 2014. Microsoft coco: Common objects in context, in: European Conference on Computer Vision, pp. 740–755. doi:10.1007/978-3-319-10602-1_48.

Lin, Y., Feng, P., Guan, J., Wang, W., Chambers, J., 2019. IENet: Interacting Embouchure One Stage Anchor Free Detector for Orientation Aerial Object Detection. arXiv e-prints. , arXiv:1912.00969.

Liu, F., Chen, R., Zhang, J., Ding, S., Liu, H., Ma, S., Xing, K., 2023. Esrtdet: An end-to-end super-resolution enhanced real-time rotated object detector for degraded aerial images. *IEEE Journal of Selected Topics in Applied Earth Observations and Remote Sensing*. 16, 4983–4998. doi:10.1109/JSTARS.2023.3278295.

Liu, K., Mattyus, G., 2015. Fast multiclass vehicle detection on aerial images. *IEEE Geoscience and Remote Sensing Letters*. 12, 1938–1942. doi:10.1109/LGRS.2015.2439517.

Liu, L., Ouyang, W., Wang, X., Fieguth, P., Chen, J., Liu, X., Pietikäinen, M., 2020. Deep learning for generic object detection: A survey. *International Journal of Computer Vision*. 128, 261–318. doi:10.1007/s11263-019-01247-4.

Liu, S., Li, F., Zhang, H., Yang, X., Qi, X., Su, H., Zhu, J., Zhang, L., 2022a. Dab-detr: Dynamic anchor boxes are better queries for detr, in: International Conference on Learning Representations.

Liu, S., Zhang, L., Lu, H., He, Y., 2022b. Center-boundary dual attention for oriented object detection in remote sensing images. *IEEE Transactions on Geoscience and Remote Sensing*. 60, 1–14. doi:10.1109/TGRS.2021.3069056.

Liu, W., Anguelov, D., Erhan, D., Szegedy, C., Reed, S., Fu, C.Y., Berg, A.C., 2016a. Ssd: Single shot multibox detector, in: European Conference on Computer Vision, pp. 21–37. doi:10.1007/978-3-319-46448-0_2.

Liu, W., Zhang, T., Huang, S., Li, K., 2022c. A hybrid optimization framework for uav reconnaissance mission planning. *Computers & Industrial Engineering*. 173, 108653. doi:10.1016/j.cie.2022.108653.

Liu, Y., Sun, P., Wergeles, N., Shang, Y., 2021a. A survey and performance evaluation of deep learning methods for small object detection. *Expert Systems with Applications*. 172, 114602. doi:10.1016/j.eswa.2021.114602.

Liu, Z., Lin, Y., Cao, Y., Hu, H., Wei, Y., Zhang, Z., Lin, S., Guo, B., 2021b. Swin transformer: Hierarchical vision transformer using shifted windows, in: IEEE/CVF International Conference on Computer Vision, pp. 9992–10002. doi:10.1109/ICCV48922.2021.00986.

Liu, Z., Mao, H., Wu, C.Y., Feichtenhofer, C., Darrell, T., Xie, S., 2022d. A convnet for the 2020s, in: IEEE/CVF Conference on Computer Vision and Pattern Recognition, pp. 11966–11976. doi:10.1109/CVPR52688.2022.01167.

Liu, Z., Wang, H., Weng, L., Yang, Y., 2016b. Ship rotated bounding box space for ship extraction from high-resolution optical satellite images with complex backgrounds. *IEEE Geoscience and Remote Sensing Letters*. 13, 1074–1078. doi:10.1109/LGRS.2016.2565705.

Long, Y., Gong, Y., Xiao, Z., Liu, Q., 2017. Accurate object localization in remote sensing images based on convolutional neural networks. *IEEE Transactions on Geoscience and Remote Sensing* 55, 2486–2498. doi:10.1109/TGRS.2016.2645610.

Lowe, D., 2004. Distinctive image features from scale-invariant keypoints. *International Journal of Computer Vision*. 60, 91–110. doi:10.1023/B:VISI.0000029664.99615.94.

Lu, D., Li, D., Li, Y., Wang, S., 2022. Oskdet: Orientation-sensitive keypoint localization for rotated object detection, in: IEEE/CVF Conference on Computer Vision and Pattern Recognition, pp. 1172–1182. doi:10.1109/CVPR52688.2022.00125.

Ma, J., Shao, W., Ye, H., Wang, L., Wang, H., Zheng, Y., Xue, X., 2018. Arbitrary-oriented scene text detection via rotation proposals. *IEEE Transactions on Multimedia*. 20, 3111–3122. doi:10.1109/TMM.2018.2818020.

Ma, T., Mao, M., Zheng, H., Gao, P., Wang, X., Han, S., Ding, E., Zhang, B., Doermann, D., 2021. Oriented Object Detection with Transformer. arXiv e-prints. , arXiv:2106.03146.

Marcos, D., Volpi, M., Komodakis, N., Tuia, D., 2017. Rotation equivariant vector field networks, in: IEEE International Conference on Computer Vision, pp. 5058–5067. doi:10.1109/ICCV.2017.540.

Mehta, S., Rastegari, M., 2021. MobileViT: Light-weight, General-purpose, and Mobile-friendly Vision Transformer. arXiv e-prints. , arXiv:2110.02178.

Ming, Q., Miao, L., Zhou, Z., Dong, Y., 2022. Cfc-net: A critical feature capturing network for arbitrary-oriented object detection in remote-sensing images. *IEEE Transactions on Geoscience and Remote Sensing*. 60, 1–14. doi:10.1109/TGRS.2021.3095186.

Ming, Q., Miao, L., Zhou, Z., Song, J., Pizurica, A., 2024. Gradient calibration loss for fast and accurate oriented bounding box regression. *IEEE Transactions on Geoscience and Remote Sensing*. 62, 1–15. doi:10.1109/TGRS.2024.3367294.

Nam, H., Ha, J.W., Kim, J., 2017. Dual attention networks for multimodal reasoning and matching, in: IEEE/CVF Conference on Computer Vision and Pattern Recognition, pp. 2156–2164. doi:10.1109/CVPR.2017.232.

Nie, G., Huang, H., 2023. Multi-oriented object detection in aerial images with double horizontal rectangles. *IEEE Transactions on Pattern Analysis and Machine Intelligence*. 45, 4932–4944. doi:10.1109/TPAMI.2022.3191753.

Osco, L.P., dos Santos de Arruda, M., Gonçalves, D.N., Dias, A., Batistot, J., de Souza, M., Gomes, F.D.G., Ramos, A.P.M., de Castro Jorge, L.A., Liesenberg, V., Li, J., Ma, L., Marcato, J., Gonçalves, W.N., 2021. A cnn approach to simultaneously count plants and detect plantation-rows from uav imagery. *ISPRS Journal of Photogrammetry and Remote Sensing*. 174, 1–17. doi:10.1016/j.isprsjprs.2021.01.024.

Pannone, S.A.A.C.C.L.F.G.R.M.M., 2022. Few-shot object detection: A survey. *ACM Computing Surveys*. , 1–37.

Pu, Y., Wang, Y., Xia, Z., Han, Y., Wang, Y., Gan, W., Wang, Z., Song, S., Huang, G., 2023. Adaptive rotated convolution for rotated object detection, in: IEEE/CVF International Conference on Computer Vision, pp. 6566–6577. doi:10.1109/ICCV51070.2023.00606.

Qian, W., Yang, X., Peng, S., Yan, J., Guo, Y., 2021. Learning modulated loss for rotated object detection, in: AAAI Conference on Artificial Intelligence, pp. 2458–2466. doi:10.1609/aaai.v35i3.16347.

Qian, W., Yang, X., Peng, S., Zhang, X., Yan, J., 2022. Rsdet++: Point-based modulated loss for more accurate rotated object detection. *IEEE Transactions on Circuits and Systems for Video Technology*. 32, 7869–7879. doi:10.1109/TCST.2022.3186070.

Qiao, S., Chen, L.C., Yuille, A., 2021. Detectors: Detecting objects with recursive feature pyramid and switchable atrous convolution, in: IEEE/CVF Conference on Computer Vision and Pattern Recognition, pp. 10208–10219. doi:10.1109/CVPR46437.2021.01008.

Qiao, Y., Miao, L., Zhou, Z., Ming, Q., 2023. A novel object detector based on high-quality rotation proposal generation and adaptive angle optimization. *IEEE Transactions on Geoscience and Remote Sensing*. 61, 1–15. doi:10.1109/TGRS.2023.3301610.

Razakarivony, S., Jurie, F., 2016. Vehicle detection in aerial imagery : A small target detection benchmark. *Journal of Visual Communication and Image Representation*. 34, 187–203. doi:10.1016/j.jvcir.2015.11.002.

Redmon, J., Divvala, S., Girshick, R., Farhadi, A., 2016. You only look once: Unified, real-time object detection, in: IEEE/CVF Conference on Computer Vision and Pattern Recognition, pp. 779–788. doi:10.1109/CVPR.2016.91.

Redmon, J., Farhadi, A., 2017. Yolo9000: Better, faster, stronger, in: IEEE/CVF Conference on Computer Vision and Pattern Recognition,

pp. 6517–6525. doi:[10.1109/CVPR.2017.690](https://doi.org/10.1109/CVPR.2017.690).

Ren, S., He, K., Girshick, R., Sun, J., 2017. Faster r-cnn: Towards real-time object detection with region proposal networks. *IEEE Transactions on Pattern Analysis and Machine Intelligence*. 39, 1137–1149. doi:[10.1109/TPAMI.2016.2577031](https://doi.org/10.1109/TPAMI.2016.2577031).

Rezatofighi, H., Tsoi, N., Gwak, J., Sadeghian, A., Reid, I., Savarese, S., 2019. Generalized intersection over union: A metric and a loss for bounding box regression, in: IEEE/CVF Conference on Computer Vision and Pattern Recognition, pp. 658–666. doi:[10.1109/CVPR.2019.00075](https://doi.org/10.1109/CVPR.2019.00075).

Russakovsky, O., Deng, J., Su, H., Krause, J., Satheesh, S., Ma, S., Huang, Z., Karpathy, A., Khosla, A., Bernstein, M., Berg, A.C., Fei-Fei, L., 2015. Imagenet large scale visual recognition challenge. *International Journal of Computer Vision*. 115, 211–252. doi:[10.1007/s11263-015-0816-y](https://doi.org/10.1007/s11263-015-0816-y).

Salvoldi, M., Cohen-Zada, A.L., Karnieli, A., 2022. Using the venus super-spectral camera for detecting moving vehicles. *ISPRS Journal of Photogrammetry and Remote Sensing*. 192, 33–48. doi:[10.1016/j.isprsjprs.2022.08.005](https://doi.org/10.1016/j.isprsjprs.2022.08.005).

Schölkopf, B., Platt, J., Hofmann, T., 2007. Analysis of representations for domain adaptation, in: Advances in Neural Information Processing Systems, pp. 137–144.

Sermeyer, J., Van Etten, A., 2019. The effects of super-resolution on object detection performance in satellite imagery, in: IEEE/CVF Conference on Computer Vision and Pattern Recognition Workshops, pp. 1432–1441. doi:[10.1109/CVPRW.2019.00184](https://doi.org/10.1109/CVPRW.2019.00184).

Sifre, L., Mallat, S., 2013. Rotation, scaling and deformation invariant scattering for texture discrimination, in: IEEE/CVF Conference on Computer Vision and Pattern Recognition, pp. 1233–1240. doi:[10.1109/CVPR.2013.163](https://doi.org/10.1109/CVPR.2013.163).

Singh, B., Davis, L.S., 2018. An analysis of scale invariance in object detection - snip, in: IEEE/CVF Conference on Computer Vision and Pattern Recognition, pp. 3578–3587. doi:[10.1109/CVPR.2018.00377](https://doi.org/10.1109/CVPR.2018.00377).

Singh, B., Najibi, M., Davis, L.S., 2018. Sniper: Efficient multi-scale training, in: Advances in Neural Information Processing Systems. URL: <https://proceedings.neurips.cc/paper/2018/file/166cee72e93a992007a89b39eb29628b-Paper.pdf>.

Song, H., Mao, H., Dally, W.J., 2016. Deep compression: Compressing deep neural networks with pruning, trained quantization and huffman coding, in: International Conference on Learning Representations.

Sun, Z., Cao, S., Yang, Y., Kitani, K., 2021. Rethinking transformer-based set prediction for object detection, in: IEEE/CVF International Conference on Computer Vision, pp. 3591–3600. doi:[10.1109/ICCV48922.2021.00359](https://doi.org/10.1109/ICCV48922.2021.00359).

Tian, Y., Zhang, M., Li, J., Li, Y., Yang, H., Li, W., 2024. Fpnformer: Rethink the method of processing the rotation-invariance and rotation-equivariance on arbitrary-oriented object detection. *IEEE Transactions on Geoscience and Remote Sensing*. 62, 1–10. doi:[10.1109/TGRS.2024.3351156](https://doi.org/10.1109/TGRS.2024.3351156).

Tong, K., Wu, Y., Zhou, F., 2020. Recent advances in small object detection based on deep learning: A review. *Image and Vision Computing*. 97, 103910. doi:[10.1016/j.imavis.2020.103910](https://doi.org/10.1016/j.imavis.2020.103910).

Tzeng, E., Hoffman, J., Saenko, K., Darrell, T., 2017. Adversarial discriminative domain adaptation, in: IEEE/CVF Conference on Computer Vision and Pattern Recognition, pp. 2962–2971. doi:[10.1109/CVPR.2017.316](https://doi.org/10.1109/CVPR.2017.316).

Vaswani, A., Shazeer, N., Parmar, N., Uszkoreit, J., Jones, L., Gomez, A.N., Kaiser, L., Polosukhin, I., 2017. Attention is all you need, in: International Conference on Neural Information Processing Systems, pp. 6000–6010.

Vinyals, O., Toshev, A., Bengio, S., Erhan, D., 2015. Show and tell: A neural image caption generator, in: IEEE/CVF Conference on Computer Vision and Pattern Recognition, pp. 3156–3164. doi:[10.1109/CVPR.2015.7298935](https://doi.org/10.1109/CVPR.2015.7298935).

Viola, P., Jones, M., 2001. Rapid object detection using a boosted cascade of simple features, in: IEEE/CVF Conference on Computer Vision and Pattern Recognition, pp. I–I. doi:[10.1109/CVPR.2001.990517](https://doi.org/10.1109/CVPR.2001.990517).

Viola, P., Jones, M., 2004. Robust real-time face detection. *International Journal of Computer Vision*. 57, 137–154. doi:[10.1023/B:VISI.0000013087.49260.fb](https://doi.org/10.1023/B:VISI.0000013087.49260.fb).

Wang, D., Zhang, Q., Xu, Y., Zhang, J., Du, B., Tao, D., Zhang, L., 2022. Advancing plain vision transformer towards remote sensing foundation model. *IEEE Transactions on Geoscience and Remote Sensing*. , 1–1doi:[10.1109/TGRS.2022.3222818](https://doi.org/10.1109/TGRS.2022.3222818).

Wang, J., Lan, C., Liu, C., Ouyang, Y., Qin, T., 2021a. Generalizing to unseen domains: A survey on domain generalization, in: International Joint Conference on Artificial Intelligence, pp. 4627–4635. doi:[10.24963/ijcai.2021/628](https://doi.org/10.24963/ijcai.2021/628).

Wang, M., Deng, W., 2018. Deep visual domain adaptation: A survey. *Neurocomputing*. 312, 135–153. doi:[10.1016/j.neucom.2018.05.083](https://doi.org/10.1016/j.neucom.2018.05.083).

Wang, P., Wu, Q., Shen, C., Dick, A., van den Hengel, A., 2018. Fvqa: Fact-based visual question answering. *IEEE Transactions on Pattern Analysis and Machine Intelligence*. 40, 2413–2427. doi:[10.1109/TPAMI.2017.2754246](https://doi.org/10.1109/TPAMI.2017.2754246).

Wang, T., Zhu, Y., Zhao, C., Zeng, W., Wang, J., Tang, M., 2021b. Adaptive class suppression loss for long-tail object detection, in: IEEE/CVF Conference on Computer Vision and Pattern Recognition, pp. 3102–3111. doi:[10.1109/CVPR46437.2021.00312](https://doi.org/10.1109/CVPR46437.2021.00312).

Wei, H., Zhang, Y., Chang, Z., Li, H., Wang, H., Sun, X., 2020. Oriented objects as pairs of middle lines. *ISPRS Journal of Photogrammetry and Remote Sensing*. 169, 268–279. doi:<https://doi.org/10.1016/j.isprsjprs.2020.09.022>.

Weiler, M., Cesa, G., 2019. General e(2)-equivariant steerable cnns, in: Advances in Neural Information Processing Systems. URL: <https://proceedings.neurips.cc/paper/2019/file/45d6637b718d0f24a237069fe41b0db4-Paper.pdf>.

Weiler, M., Hamprecht, F.A., Storath, M., 2018. Learning steerable filters for rotation equivariant cnns, in: IEEE/CVF Conference on Computer Vision and Pattern Recognition, pp. 849–858. doi:[10.1109/CVPR.2018.00095](https://doi.org/10.1109/CVPR.2018.00095).

Wen, L., Du, D., Zhu, P., Hu, Q., Wang, Q., Bo, L., Lyu, S., 2021. Detection, tracking, and counting meets drones in crowds: A benchmark, in: IEEE/CVF Conference on Computer Vision and Pattern Recognition, pp. 7808–7817. doi:[10.1109/CVPR46437.2021.00772](https://doi.org/10.1109/CVPR46437.2021.00772).

Worrall, D.E., Garbin, S.J., Turmukhambetov, D., Brostow, G.J., 2017. Harmonic networks: Deep translation and rotation equivariance, in: IEEE/CVF Conference on Computer Vision and Pattern Recognition, pp. 7168–7177. doi:[10.1109/CVPR.2017.758](https://doi.org/10.1109/CVPR.2017.758).

Wright, J., Yang, A.Y., Ganesh, A., Sastry, S.S., Ma, Y., 2009. Robust face recognition via sparse representation. *IEEE Transactions on Pattern Analysis and Machine Intelligence*. 31, 210–227. doi:[10.1109/TPAMI.2008.79](https://doi.org/10.1109/TPAMI.2008.79).

Wu, X., Li, W., Hong, D., Tao, R., Du, Q., 2022. Deep learning for unmanned aerial vehicle-based object detection and tracking: A survey. *IEEE Geoscience and Remote Sensing Magazine*. 10, 91–124. doi:[10.1109/MGRS.2021.3115137](https://doi.org/10.1109/MGRS.2021.3115137).

Wu, X., Sahoo, D., Hoi, S.C., 2020. Recent advances in deep learning for object detection. *Neurocomputing*. 396, 39–64. doi:[10.1016/j.neucom.2020.01.085](https://doi.org/10.1016/j.neucom.2020.01.085).

Xia, G.S., Bai, X., Ding, J., Zhu, Z., Belongie, S., Luo, J., Datcu, M., Pelillo, M., Zhang, L., 2018. Dota: A large-scale dataset for object detection in aerial images, in: IEEE/CVF Conference on Computer Vision and Pattern Recognition, pp. 3974–3983. doi:[10.1109/CVPR.2018.00418](https://doi.org/10.1109/CVPR.2018.00418).

Xiao, Z., Liu, Q., Tang, G., Zhai, X., 2015. Elliptic fourier transformation-based histograms of oriented gradients for rotationally invariant object detection in remote-sensing images. *International Journal of Remote Sensing* 36, 618–644. doi:[10.1080/01431161.2014.999881](https://doi.org/10.1080/01431161.2014.999881).

Xiao, Z., Qian, L., Shao, W., Tan, X., Wang, K., 2020. Axis learning for orientated objects detection in aerial images. *Remote Sensing*. 12, doi:[10.3390/rs12060908](https://doi.org/10.3390/rs12060908).

Xie, S., Girshick, R., Dollár, P., Tu, Z., He, K., 2017. Aggregated residual transformations for deep neural networks, in: IEEE/CVF Conference on Computer Vision and Pattern Recognition, pp. 5987–5995. doi:[10.1109/CVPR.2017.634](https://doi.org/10.1109/CVPR.2017.634).

Xie, X., Cheng, G., Wang, J., Yao, X., Han, J., 2021. Oriented r-cnn for object detection, in: IEEE/CVF International Conference on Computer Vision, pp. 3500–3509. doi:10.1109/ICCV48922.2021.00350.

Xiong, Y., Liu, H., Gupta, S., Akin, B., Bender, G., Wang, Y., Kindermans, P.J., Tan, M., Singh, V., Chen, B., 2021. Mobiledets: Searching for object detection architectures for mobile accelerators, in: IEEE/CVF Conference on Computer Vision and Pattern Recognition, pp. 3824–3833. doi:10.1109/CVPR46437.2021.00382.

Xu, C., Ding, J., Wang, J., Yang, W., Yu, H., Yu, L., Xia, G.S., 2023. Dynamic coarse-to-fine learning for oriented tiny object detection, in: IEEE/CVF Conference on Computer Vision and Pattern Recognition, pp. 7318–7328. doi:10.1109/CVPR52729.2023.00707.

Xu, Y., Fu, M., Wang, Q., Wang, Y., Chen, K., Xia, G.S., Bai, X., 2021a. Gliding vertex on the horizontal bounding box for multi-oriented object detection. *IEEE Transactions on Pattern Analysis and Machine Intelligence*. 43, 1452–1459. doi:10.1109/TPAMI.2020.2974745.

Xu, Y., Zhang, Q., Zhang, J., Tao, D., 2021b. Vitae: Vision transformer advanced by exploring intrinsic inductive bias, in: Advances in Neural Information Processing Systems. URL: https://openreview.net/pdf?id=_RnHyIeu5Y5.

Yang, X., Hou, L., Zhou, Y., Wang, W., Yan, J., 2021a. Dense label encoding for boundary discontinuity free rotation detection, in: IEEE/CVF Conference on Computer Vision and Pattern Recognition, pp. 15814–15824. doi:10.1109/CVPR46437.2021.01556.

Yang, X., Sun, H., Fu, K., Yang, J., Sun, X., Yan, M., Guo, Z., 2018. Automatic ship detection in remote sensing images from google earth of complex scenes based on multiscale rotation dense feature pyramid networks. *Remote Sensing*. 10. doi:10.3390/rs10010132.

Yang, X., Yan, J., 2020. Arbitrary-oriented object detection with circular smooth label, in: European Conference on Computer Vision, pp. 677–694. doi:10.1007/978-3-030-58598-3_40.

Yang, X., Yan, J., Feng, Z. and He, T., 2021b. R3det: Refined single-stage detector with feature refinement for rotating object, in: AAAI Conference on Artificial Intelligence, pp. 3163–3171. doi:10.1609/aaai.v35i14.16426.

Yang, X., Yan, J., Liao, W., Yang, X., Tang, J., He, T., 2022a. Scrdet++: Detecting small, cluttered and rotated objects via instance-level feature denoising and rotation loss smoothing. *IEEE Transactions on Pattern Analysis and Machine Intelligence*. , 1–1doi:10.1109/TPAMI.2022.3166956.

Yang, X., Yan, J., Ming, Q., Wang, W., Zhang, X., Tian, Q., 2021c. Rethinking rotated object detection with gaussian wasserstein distance loss, in: International Conference on Machine Learning, pp. 11830–11841. URL: <https://proceedings.mlr.press/v139/yang21l.html>.

Yang, X., Yang, J., Yan, J., Zhang, Y., Zhang, T., Guo, Z., Sun, X., Fu, K., 2019a. Scrdet: Towards more robust detection for small, cluttered and rotated objects, in: IEEE/CVF International Conference on Computer Vision, pp. 8231–8240. doi:10.1109/ICCV.2019.00832.

Yang, X., Yang, X., Yang, J., Ming, Q., Wang, W., Tian, Q., Yan, J., 2021d. Learning high-precision bounding box for rotated object detection via kullback-leibler divergence, in: Advances in Neural Information Processing Systems, pp. 18381–18394. URL: <https://proceedings.neurips.cc/paper/2021/file/98f13708210194c475687be6106a3b84-Paper.pdf>.

Yang, X., Zhang, G., Yang, X., Zhou, Y., Wang, W., Tang, J., He, T., Yan, J., 2022b. Detecting rotated objects as gaussian distributions and its 3-d generalization. *IEEE Transactions on Pattern Analysis and Machine Intelligence*. , 1–18doi:10.1109/TPAMI.2022.3197152.

Yang, X., Zhou, Y., Zhang, G., Yang, J., Wang, W., Yan, J., Zhang, X., Tian, Q., 2022. The KFloU Loss for Rotated Object Detection. arXiv e-prints. , arXiv:2201.12558.

Yang, Z., Liu, S., Hu, H., Wang, L., Lin, S., 2019b. Reppoints: Point set representation for object detection, in: IEEE/CVF International Conference on Computer Vision, pp. 9656–9665. doi:10.1109/ICCV.2019.00975.

Yao, Y., Cheng, G., Wang, G., Li, S., Zhou, P., Xie, X., Han, J., 2023. On improving bounding box representations for oriented object detection. *IEEE Transactions on Geoscience and Remote Sensing*. 61, 1–11. doi:10.1109/TGRS.2022.3231340.

Ye, Q., Doermann, D., 2015. Text detection and recognition in imagery: A survey. *IEEE Transactions on Pattern Analysis and Machine Intelligence*. 37, 1480–1500. doi:10.1109/TPAMI.2014.2366765.

Yi, J., Wu, P., Liu, B., Huang, Q., Qu, H., Metaxas, D., 2021. Oriented object detection in aerial images with box boundary-aware vectors, in: IEEE Winter Conference on Applications of Computer Vision, pp. 2149–2158. doi:10.1109/WACV48630.2021.00220.

Yin, X.C., Zuo, Z.Y., Tian, S., Liu, C.L., 2016. Text detection, tracking and recognition in video: A comprehensive survey. *IEEE Transactions on Image Processing*. 25, 2752–2773. doi:10.1109/TIP.2016.2554321.

Yosinski, J., Clune, J., Bengio, Y., Lipson, H., 2014. How transferable are features in deep neural networks?, in: International Conference on Neural Information Processing Systems - Volume 2, p. 3320–3328. doi:10.5555/2969033.2969197.

Yu, H., Tian, Y., Ye, Q., Liu, Y., 2023. Spatial Transform Decoupling for Oriented Object Detection. arXiv e-prints. doi:10.48550/arXiv.2308.10561.

Yu, Y., Da, F., 2023. Phase-shifting coder: Predicting accurate orientation in oriented object detection, in: IEEE/CVF Conference on Computer Vision and Pattern Recognition, pp. 13354–13363. doi:10.1109/CVPR52729.2023.01283.

Zafeiriou, S., Zhang, C., Zhang, Z., 2015. A survey on face detection in the wild: Past, present and future. *Computer Vision and Image Understanding*. 138, 1–24. doi:10.1016/j.cviu.2015.03.015.

Zeng, Y., Chen, Y., Yang, X., Li, Q., Yan, J., 2024. Ars-detr: Aspect ratio-sensitive detection transformer for aerial oriented object detection. *IEEE Transactions on Geoscience and Remote Sensing*. 62, 1–15. doi:10.1109/TGRS.2024.3364713.

Zhang, C., Yang, Z., He, X., Deng, L., 2020a. Multimodal intelligence: Representation learning, information fusion, and applications. *IEEE Journal of Selected Topics in Signal Processing*. 14, 478–493. doi:10.1109/JSTSP.2020.2987728.

Zhang, D., Han, J., Cheng, G., Yang, M.H., 2022a. Weakly supervised object localization and detection: A survey. *IEEE Transactions on Pattern Analysis and Machine Intelligence*. 44, 5866–5885. doi:10.1109/TPAMI.2021.3074313.

Zhang, F., Wang, X., Zhou, S., Wang, Y., Hou, Y., 2022b. Arbitrary-oriented ship detection through center-head point extraction. *IEEE Transactions on Geoscience and Remote Sensing*. 60, 1–14. doi:10.1109/TGRS.2021.3120411.

Zhang, H., Li, F., Liu, S., Zhang, L., Su, H., Zhu, J., Ni, L.M., Shum, H.Y., 2022. DINO: DETR with Improved DeNoising Anchor Boxes for End-to-End Object Detection. arXiv e-prints. doi:10.48550/arXiv.2203.03605.

Zhang, J., Lei, J., Xie, W., Fang, Z., Li, Y., Du, Q., 2023a. Superyolo: Super resolution assisted object detection in multimodal remote sensing imagery. *IEEE Transactions on Geoscience and Remote Sensing* 61, 1–15. doi:10.1109/TGRS.2023.3258666.

Zhang, Q., Xu, Y., Zhang, J., Tao, D., 2023b. Vitaev2: Vision transformer advanced by exploring inductive bias for image recognition and beyond. *International Journal of Computer Vision*. , 1573–1405doi:10.1007/s11263-022-01739-w.

Zhang, S., Chi, C., Yao, Y., Lei, Z., Li, S.Z., 2020b. Bridging the gap between anchor-based and anchor-free detection via adaptive training sample selection, in: IEEE/CVF Conference on Computer Vision and Pattern Recognition, pp. 9756–9765. doi:10.1109/CVPR42600.2020.00978.

Zhang, T., Zhang, X., Liu, C., Shi, J., Wei, S., Ahmad, I., Zhan, X., Zhou, Y., Pan, D., Li, J., Su, H., 2021a. Balance learning for ship detection from synthetic aperture radar remote sensing imagery. *ISPRS Journal of Photogrammetry and Remote Sensing*. 182, 190–207. doi:10.1016/j.isprsjprs.2021.10.010.

Zhang, T., Zhang, X., Zhu, P., Chen, P., Tang, X., Li, C., Jiao, L., 2022. Foreground refinement network for rotated object detection in remote sensing images. *IEEE Transactions on Geoscience and Remote Sensing*. 60, 1–13. doi:10.1109/TGRS.2021.3109145.

Zhang, X., Zhang, T., Wang, G., Zhu, P., Tang, X., Jia, X., Jiao, L., 2023. Remote Sensing Object Detection Meets Deep Learning: A Meta-review of Challenges and Advances. arXiv e-prints. .

Zhang, Y., Yuan, Y., Feng, Y., Lu, X., 2019. Hierarchical and robust convolutional neural network for very high-resolution remote sensing object detection. *IEEE Transactions on Geoscience and Remote Sensing*. 57, 5535–5548. doi:10.1109/TGRS.2019.2900302.

Zhang, Z., Guo, W., Zhu, S., Yu, W., 2018. Toward arbitrary-oriented ship detection with rotated region proposal and discrimination networks. *IEEE Geoscience and Remote Sensing Letters*. 15, 1745–1749. doi:10.1109/LGRS.2018.2856921.

Zhang, Z., Zhang, L., Wang, Y., Feng, P., He, R., 2021b. Shipsimagenet: A large-scale fine-grained dataset for ship detection in high-resolution optical remote sensing images. *IEEE Journal of Selected Topics in Applied Earth Observations and Remote Sensing*. 14, 8458–8472. doi:10.1109/JSTARS.2021.3104230.

Zhao, F., Xia, L., Kylling, A., Li, R., Shang, H., Xu, M., 2018. Detection flying aircraft from landsat 8 oli data. *ISPRS Journal of Photogrammetry and Remote Sensing*. 141, 176–184. doi:10.1016/j.isprsjprs.2018.05.001.

Zhao, P., Qu, Z., Bu, Y., Tan, W., Guan, Q., 2021. Polardet: a fast, more precise detector for rotated target in aerial images. *International Journal of Remote Sensing*. 42, 5831–5861. doi:10.1080/01431161.2021.1931535.

Zhao, Z.Q., Zheng, P., Xu, S.T., Wu, X., 2019. Object detection with deep learning: A review. *IEEE Transactions on Neural Networks and Learning Systems*. 30, 3212–3232. doi:10.1109/TNNLS.2018.2876865.

Zheng, Y., Sun, P., Zhou, Z., Xu, W., Ren, Q., 2021. Adt-det: Adaptive dynamic refined single-stage transformer detector for arbitrary-oriented object detection in satellite optical imagery. *Remote Sensing* 13. doi:10.3390/rs13132623.

Zheng, Z., Wang, P., Liu, W., Li, J., Ye, R., Ren, D., 2020. Distance-iou loss: Faster and better learning for bounding box regression, in: AAAI Conference on Artificial Intelligence, pp. 12993–13000. doi:10.1609/aaai.v34i07.6999.

Zhou, L., Wei, H., Li, H., Zhao, W., Zhang, Y., Zhang, Y., 2020. Arbitrary-oriented object detection in remote sensing images based on polar coordinates. *IEEE Access*. 8, 223373–223384. doi:10.1109/ACCESS.2020.3041025.

Zhou, X., Zhuo, J., Krähenbühl, P., 2019. Bottom-up object detection by grouping extreme and center points, in: IEEE/CVF Conference on Computer Vision and Pattern Recognition, pp. 850–859. doi:10.1109/CVPR.2019.00094.

Zhou, Y., Yang, X., Zhang, G., Wang, J., Liu, Y., Hou, L., Jiang, X., Liu, X., Yan, J., Lyu, C., Zhang, W., Chen, K., 2022. Mmrotate: A rotated object detection benchmark using pytorch, in: ACM International Conference on Multimedia, pp. 7331–7334. doi:10.1145/3503161.3548541.

Zhou, Y., Ye, Q., Qiu, Q., Jiao, J., 2017. Oriented response networks, in: IEEE/CVF Conference on Computer Vision and Pattern Recognition, pp. 4961–4970. doi:10.1109/CVPR.2017.527.

Zhu, H., Chen, X., Dai, W., Fu, K., Ye, Q., Jiao, J., 2015. Orientation robust object detection in aerial images using deep convolutional neural network, in: 2015 IEEE International Conference on Image Processing, pp. 3735–3739. doi:10.1109/ICIP.2015.7351502.

Zhu, M., Pan, P., Chen, W., Yang, Y., 2019. Dm-gan: Dynamic memory generative adversarial networks for text-to-image synthesis, in: IEEE/CVF Conference on Computer Vision and Pattern Recognition, pp. 5795–5803. doi:10.1109/CVPR.2019.00595.

Zhu, X., Su, W., Lu, L., Li, B., Wang, X., Dai, J., 2021. Deformable detr: Deformable transformers for end-to-end object detection, in: International Conference on Learning Representations.

Zhu, Y., Du, J., Wu, X., 2020. Adaptive period embedding for representing oriented objects in aerial images. *IEEE Transactions on Geoscience and Remote Sensing*. 58, 7247–7257. doi:10.1109/TGRS.2020.2981203.

Zou, Z., Chen, K., Shi, Z., Guo, Y., Ye, J., 2023. Object detection in 20 years: A survey. *Proceedings of the IEEE*. 111, 257–276. doi:10.1109/JPROC.2023.3238524.

Zou, Z., Shi, Z., 2018. Random access memories: A new paradigm for target detection in high resolution aerial remote sensing images. *IEEE Transactions on Image Processing*. 27, 1100–1111. doi:10.1109/TIP.2017.2773199.

A. θ -based Representation

The θ -based representation adopts a vector in the format of (x, y, w, h, θ) to define an OBB. The present approaches can be classified into two types according to the definition of the angle θ , including (which follows the OpenCV protocol) and the long edge definition. As shown in Figure 9(a), the former defines θ as the acute (or right) angle between the OBB and x -axis, leading to $\theta \in (0, \frac{\pi}{2}]$. Note that the width w is defined as the side of the acute angle and can be shorter than the height h , which is shown at the top of Figure 9(a). To tackle this issue, the long edge definition is proposed by setting θ as the angle between the long edge of the OBB and x -axis. Therefore, the angular range is $[-\frac{\pi}{2}, \frac{\pi}{2})$ (Ding et al., 2019; Han et al., 2021a) or $[-\frac{\pi}{4}, \frac{3\pi}{4})$ (Han et al., 2022), which are shown in Figure 9(b) and Figure 9(c), respectively. As shown in the bottom of Figure 9, the parameters of the same OBB have significant differences in different OBB representations.

Built upon well-designed horizontal detectors, most oriented object detectors predict OBBs in a regression fashion. In the θ -based OBB representation, given an anchor box denoted by $b_a = (x_a, y_a, w_a, h_a, \theta_a)$, the neural network first predicts the offsets between the predicted OBB and the anchor box:

$$\begin{aligned} t_x^p &= \frac{x_p - x_a}{w_a}, t_y^p = \frac{y_p - y_a}{h_a}, \\ t_w^p &= \log \frac{w_p}{w_a}, t_h^p = \log \frac{h_p}{h_a}, t_\theta^p = f\left(\frac{\theta_p - \theta_a}{\pi}\right) \end{aligned} \quad (6)$$

where $b_p = (x_p, y_p, w_p, h_p, \theta_p)$ denotes the predicted OBB. $f(\cdot)$ is used to ensure that the angle difference stays within the preset range, thus avoiding the impact of PoA. Similarly, the GT offsets are denoted by:

$$\begin{aligned} t_x^g &= \frac{x_g - x_a}{w_a}, t_y^g = \frac{y_g - y_a}{h_a}, \\ t_w^g &= \log \frac{w_g}{w_a}, t_h^g = \log \frac{h_g}{h_a}, t_\theta^g = f\left(\frac{\theta_g - \theta_a}{\pi}\right) \end{aligned} \quad (7)$$

where $b_g = (x_g, y_g, w_g, h_g, \theta_g)$ denotes the GT OBB. Hence, the objective function for the regression task is:

$$L_{reg} = \sum_{i \in \{x, y, w, h, \theta\}} L_n(t_i^p - t_i^g) \quad (8)$$

where $L_n(\cdot)$ denotes the L_n norm and the smooth L_1 loss (Girshick, 2015) is widely adopted. Due to the PoA (Qian et al., 2021, 2022; Yang et al., 2021c, 2022b), the OBB regression will encounter the following challenges.

(1) **Inconsistency between Metric and Loss.** Although the majority of detectors adopt the smooth L1 loss as the objective function of regression, the most commonly used metric for localization is RIoU. Therefore, there is an inconsistency between the loss function and the evaluation metric. This implies that an optimum choice for the regression task may not guarantee a high localization accuracy in terms of RIoU. What's more, a good regression loss function should

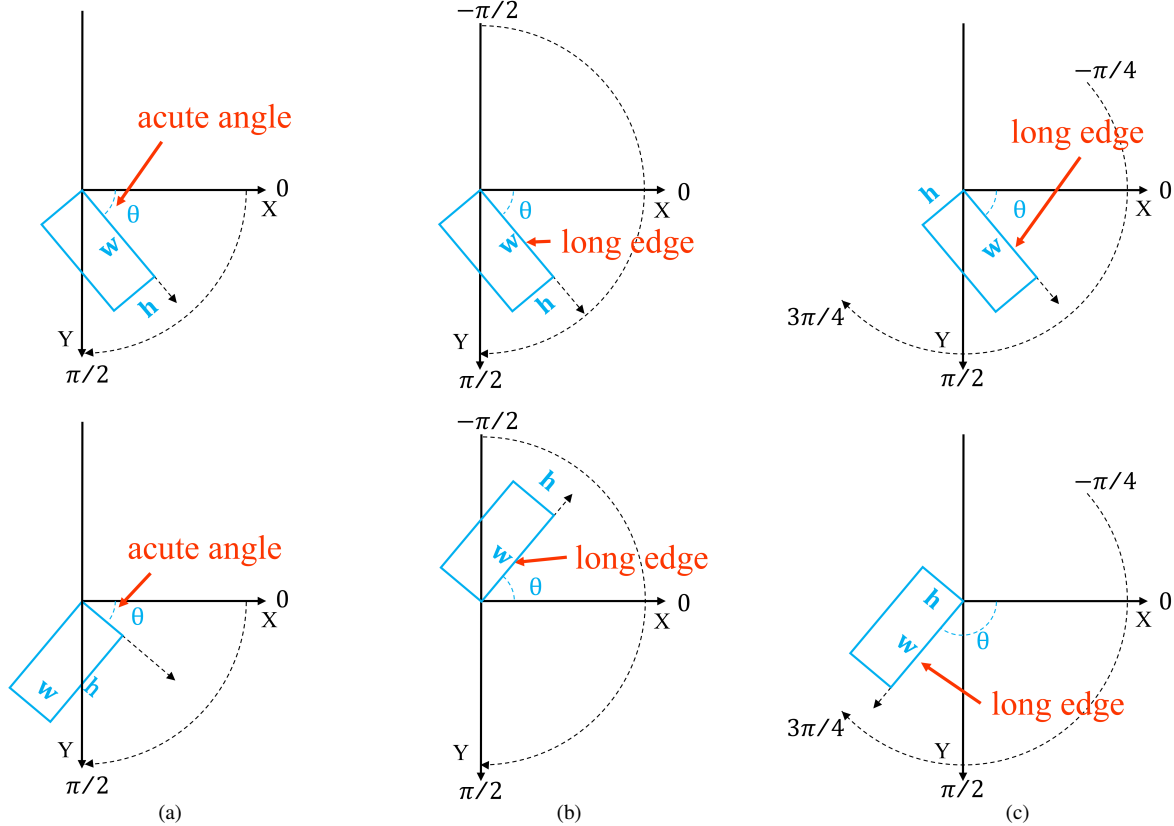


Figure 9: Definition of θ -based representation. The OBBs depicted in the top/bottom row are the same. (a) OpenCV Definition ($\theta \in (0, \frac{\pi}{2}]$) (**Top**: height is longer than width. **Bottom**: width is longer than height). (b) Long edge definition with an angular range of $[-\frac{\pi}{2}, \frac{\pi}{2}]$. (c) Long edge definition with an angular range of $[-\frac{\pi}{4}, \frac{3\pi}{4}]$.

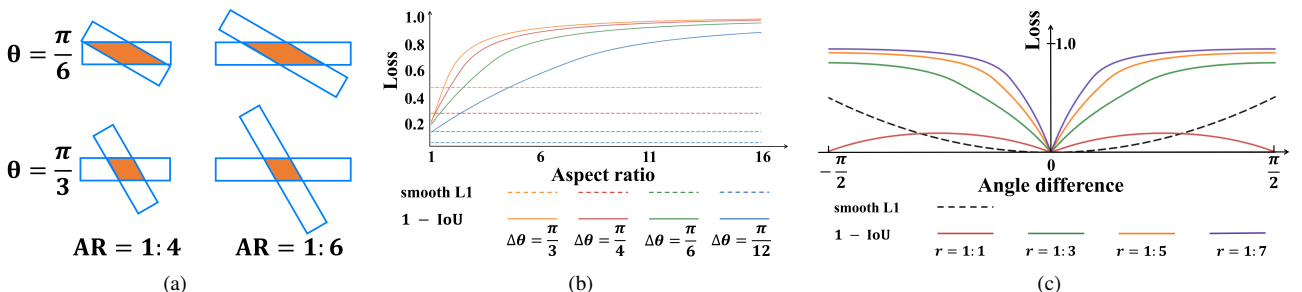


Figure 10: Comparison between metric and loss (Qian et al., 2021, 2022; Yang et al., 2021c). (a) A sketch of RIoU change caused by angle and aspect ratio (AR) variation. (b) and (c) depict the changes of the regression loss and RIoU with aspect ratio and angle difference, respectively.

take into account the central point distance, aspect ratio, and overlap area, which has been demonstrated to be effective in horizontal object detection (Rezatofighi et al., 2019; Zheng et al., 2020). However, the aspect ratio and the overlap area can be disregarded by the smooth L1 loss easily.

We illustrate the inconsistency between metric and loss in Figure 10. As shown in Figure 10(a), the top and the bottom rows have different angle differences, while the aspect ratio of the OBBs on the left is different from those on the right. Meanwhile, the center points, width, and height of the

four cases are the same. The orange area denotes the IoU between OBBs. Note that the regression loss is sensitive to angle variances but remains unchanged for different aspect ratios. Specifically, when the aspect ratio varies, the union of two OBBs will change but the intersection is constant, causing the change of RIoU. The same conclusion can be drawn from Figure 10(b), which shows the variation curves of the RIoU and smooth L1 loss w.r.t aspect ratio under different angle differences. Note that the RIoU changes drastically but the smooth L1 loss remains constant. Furthermore, Figure

10(c) shows the variation curve of RIoU and smooth L1 loss with respect to the angle under different aspect ratios. In the neighborhood of 0, both losses are consistent in monotonicity but not in convexity. The RIoU changes more intensely than the smooth L1 loss when the angle difference is close to zero.

(2) Angular Boundary Discontinuity and Square-like Problem

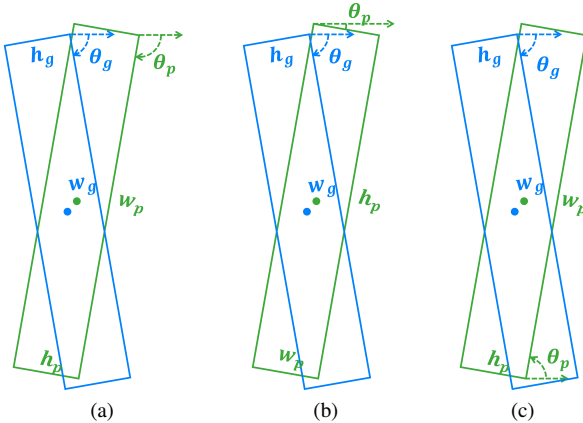


Figure 11: Illustration of angular boundary discontinuity (Yang et al., 2021c). The predicted and GT OBB are represented by green and blue, respectively. (a) The ideal form of OBB representation. The two OBBs only differ slightly in terms of the angle and center point. (b) OBB representation with OpenCV definition, encountering PoA and exchangeability of edges (EoE). (c) OBB representation with long edge definition, encountering a significant angle difference.

Because of the PoA problem (Yang et al., 2021c,d; Yang et al., 2022; Qian et al., 2021, 2022), the smooth L1 loss suffers from the problem of angular boundary discontinuity, which is illustrated in Figure 11. Specifically, a small angle difference may cause a large loss change when the angular value approaches the angular boundary range. Figure 11(a) illustrates an ideal OBB representation, where the predicted and GT OBB only differ slightly in terms of the angle and center point. For OBBs with OpenCV definition, the angular value must be an acute or right angle, *i.e.*, $\theta \in (0, \frac{\pi}{2}]$, as shown in Figure 11(b). As a result, the angle difference between the two OBBs increases sharply as the angular value is close to 0 or $\frac{\pi}{2}$. In addition, the width of the predicted OBB is the short edge, whereas the width of the GT OBB is the long edge, causing a significant regression loss of width and height. For OBBs under long edge definition with the angular range of $[-\frac{\pi}{2}, \frac{\pi}{2})$, the angular boundary discontinuity leads to a significant angle difference, *i.e.*, $|\theta_g - \theta_p| \approx \pi$, as shown in Figure 11(c). This problem will also occur in long edge definition with the angular range of $[-\frac{\pi}{4}, \frac{3\pi}{4})$ when the angular value is close to $-\frac{\pi}{4}$ or $\frac{3\pi}{4}$.

For square-like objects, including storage-tank and roundabouts, the long edge definition will encounter a so-called square-like problem due to the difference of angle parameters (Yang et al., 2021c,d; Yang et al., 2022). As shown in

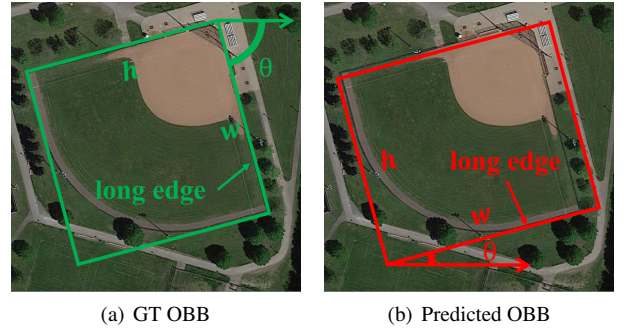


Figure 12: Illustration of the square-like problem (Yang et al., 2021c,a).

Figure 12, when the aspect ratio is close to 1 but the length and width of the predicted OBB are opposite to that of GT, the corresponding angle will differ by about $\frac{\pi}{2}$, leading to a large regression loss even if the RIoU is about 1.

B. Quadrilateral Representation

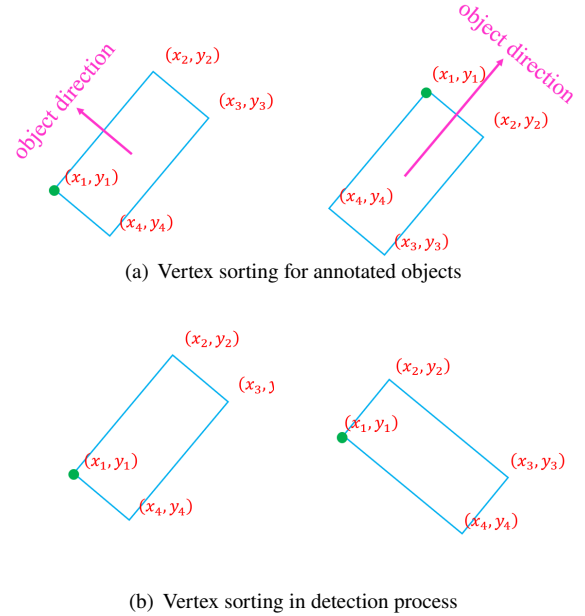


Figure 13: Definition of quadrilateral representation. **Top:** the top-left vertex relative to the object orientation is chosen as the start point. **Bottom:** the leftmost vertex is chosen as the starting point.

The quadrilateral representation denotes an OBB as a vector $(x_1, y_1, x_2, y_2, x_3, y_3, x_4, y_4)$, where (x_i, y_i) indicates the image coordinates of the i_{th} vertex arranged in a clockwise order (Xu et al., 2021a). This representation method can compactly enclose oriented objects with large deformation and has been widely adopted to annotate objects in large-scale RS datasets, including DOTA (Xia et al., 2018; Ding et al., 2022), and HRSC2016 (Liu et al., 2016b). Significantly, the top-left vertex relative to the object orientation

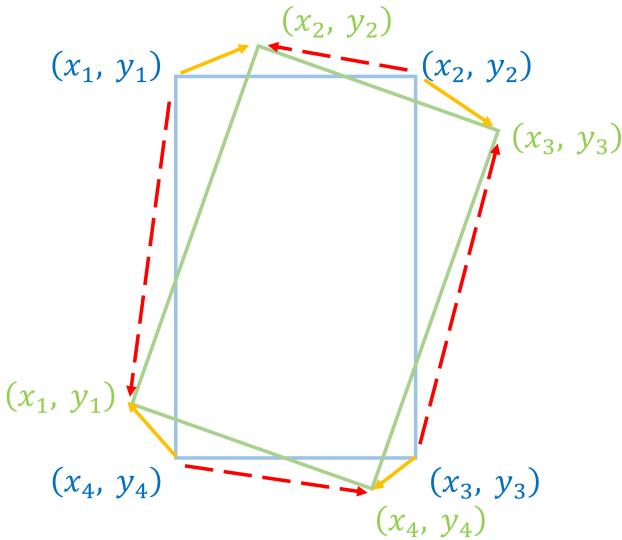


Figure 14: Illustration of vertexes sorting problem. The dashed line and solid line represent the actual and ideal regression forms, respectively.

is chosen as the starting point (x_1, y_1) , as shown in Figure 13(a).

For the quadrilateral representation, the detector outputs a vector $(\Delta x_1^p, \Delta y_1^p, \Delta x_2^p, \Delta y_2^p, \Delta x_3^p, \Delta y_3^p, \Delta x_4^p, \Delta y_4^p)$, where $(\Delta x_i^p, \Delta y_i^p)$ represent the relative offsets between the i -th vertex of the predicted OBB and the corresponding anchor box. Then, the predicted offsets are used to approximate the GT coordinate offsets $(\Delta x_1^g, \Delta y_1^g, \Delta x_2^g, \Delta y_2^g, \Delta x_3^g, \Delta y_3^g, \Delta x_4^g, \Delta y_4^g)$ between the i -th vertex of the GT OBB and that of the anchor box. The regression loss of quadrilateral OBB representation can be expressed as:

$$L_{reg} = \sum_{i=1}^4 [L_n(\Delta x_i^p - \Delta x_i^g) + L_n(\Delta y_i^p - \Delta y_i^g)] \quad (9)$$

Generally, the anchor box selects the top-left vertex in the image as the starting point. To ensure consistency, the leftmost vertexes of the predicted OBB and the corresponding GT OBB are chosen as the starting point, as shown in Figure 13(b). However, the inappropriate vertex sorting may cause inconsistencies between the vertex sequences of the anchor and the GT OBB, which is known as the vertexes sorting problem or the corners sorting problem (Qian et al., 2021, 2022; Xu et al., 2021a). Figure 14 shows a case of the problem. The anchor and the GT OBB are shown in blue and green respectively, and the dashed line and the solid line denote the actual and ideal vertexes matching during regression. In the ideal setting, the vertexes matching from the anchor to the GT is: $(x_1, y_1) \rightarrow (x_2, y_2), (x_2, y_2) \rightarrow (x_3, y_3), (x_3, y_3) \rightarrow (x_4, y_4), (x_4, y_4) \rightarrow (x_1, y_1)$. However, in the actual regression, the vertexes matching is: $(x_1, y_1) \rightarrow (x_1, y_1), (x_2, y_2) \rightarrow (x_2, y_2), (x_3, y_3) \rightarrow (x_3, y_3), (x_4, y_4) \rightarrow (x_4, y_4)$. Such inconsistency causes a large regression loss, confusing the network during the training

process. Hence, it is critical to determine the sequence of vertexes in advance to stabilize the training process.

C. Datasets

In Table 2 of our main paper, we review a series of benchmarks regarding oriented object detection. However, space constraints prevent us from presenting all of them in detail. In this section, further details regarding the datasets mentioned in Section 7.1 are presented.

SZTAKI-INRIA (Benedek et al., 2012) contains 665 buildings in 9 multi-sensor aerial or satellite images taken from different cities. Due to the small capacity, this dataset is used to evaluate traditional object detection algorithms.

3K vehicle (Liu and Mattyus, 2015) is created for vehicle detection, comprising 20 images and 14,235 vehicles. The images have a resolution of 5616×3744 and are captured by a DLR camera system at a height of 1,000m above the ground. Therefore, the ground sample distance (GSD) is approximately 13 cm, leading to smaller scale variations. Besides, the images have a similar background. Hence, this dataset is excluded from the evaluation of algorithms on complicated scenes.

VEDAI (Razakarivony and Jurie, 2016) is also proposed for vehicle detection, containing more categories and a wider variety of backgrounds, *e.g.*, fields, grass, mountains, urban area, etc, making the detection more complicated. It comprises 1,210 images with a resolution of $1,024 \times 1,024$. The images are cropped from Very-High-Resolution (VHR) satellite images with a GSD of 12.5cm. However, the dataset only consists of 3,640 instances, because the images with too many dense vehicles are excluded. It is worth mentioning that each image has four color channels, including three visible channels and one 8-bit near-infrared channel.

UCAS-AOD (Zhu et al., 2015) contains 7,482 planes in 1,000 images, 7,114 cars in 510 images, and 910 negative images. All images in this dataset are cropped from Google Earth aerial images. Especially, the instances are carefully selected to ensure their orientations are distributed evenly.

DOTA (Xia et al., 2018; Ding et al., 2022). Figure 15 shows the number of instances for each category in training and validation subsets of DOTA-V1.0, V1.5, and V2.0. Note that the distributions of different categories are severely imbalanced. The instances of small-vehicle and ship have a large quantity, while nearly half of the other categories have quantities of less than 1,000, including plane, baseball diamond, ground track field, basketball court, soccer ball field, roundabout, helicopter, container crane, airport and helipad. The severe category imbalance makes the model seriously over-fitting to the many-shot categories but under-fitting to the low-shot categories (Gupta et al., 2019; Cui et al., 2019; Wang et al., 2021b). Figure 16 further summarizes the size and ratio distributions for each category in three versions of DOTA, respectively. As shown in Figure 16(a), the minimum size is 3 – 4 orders of magnitude lower than the maximum size in each category. Moreover, there is also a large range of size differences between categories.

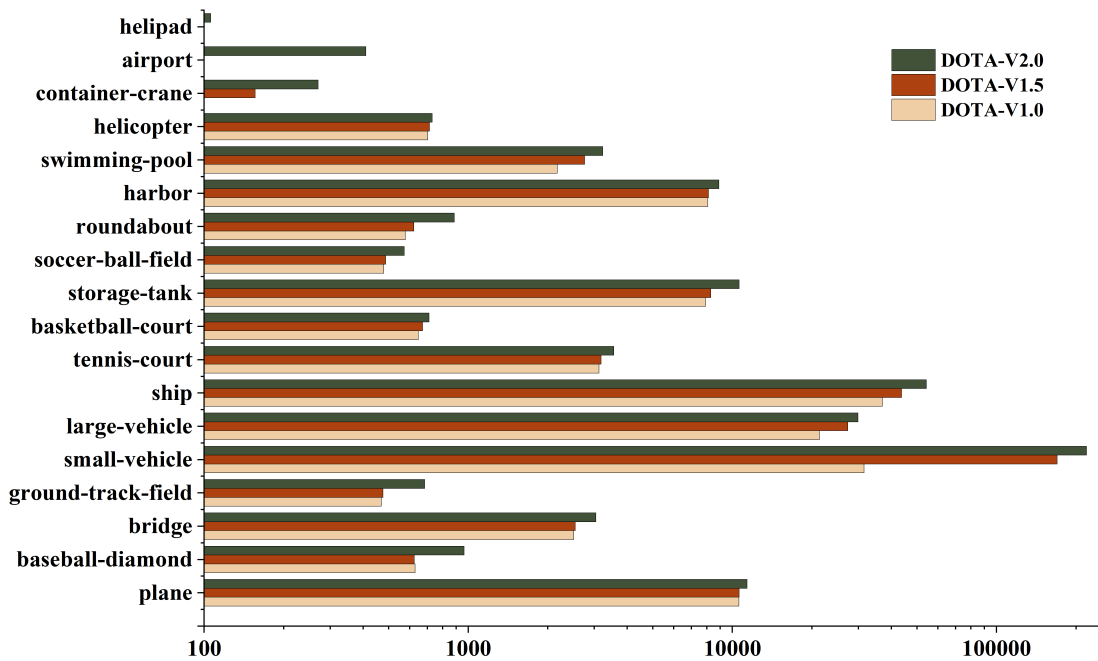


Figure 15: Number of instances for each category in training and validation subsets of DOTA-V1.0, V1.5, and V2.0 (Xia et al., 2018; Ding et al., 2022)

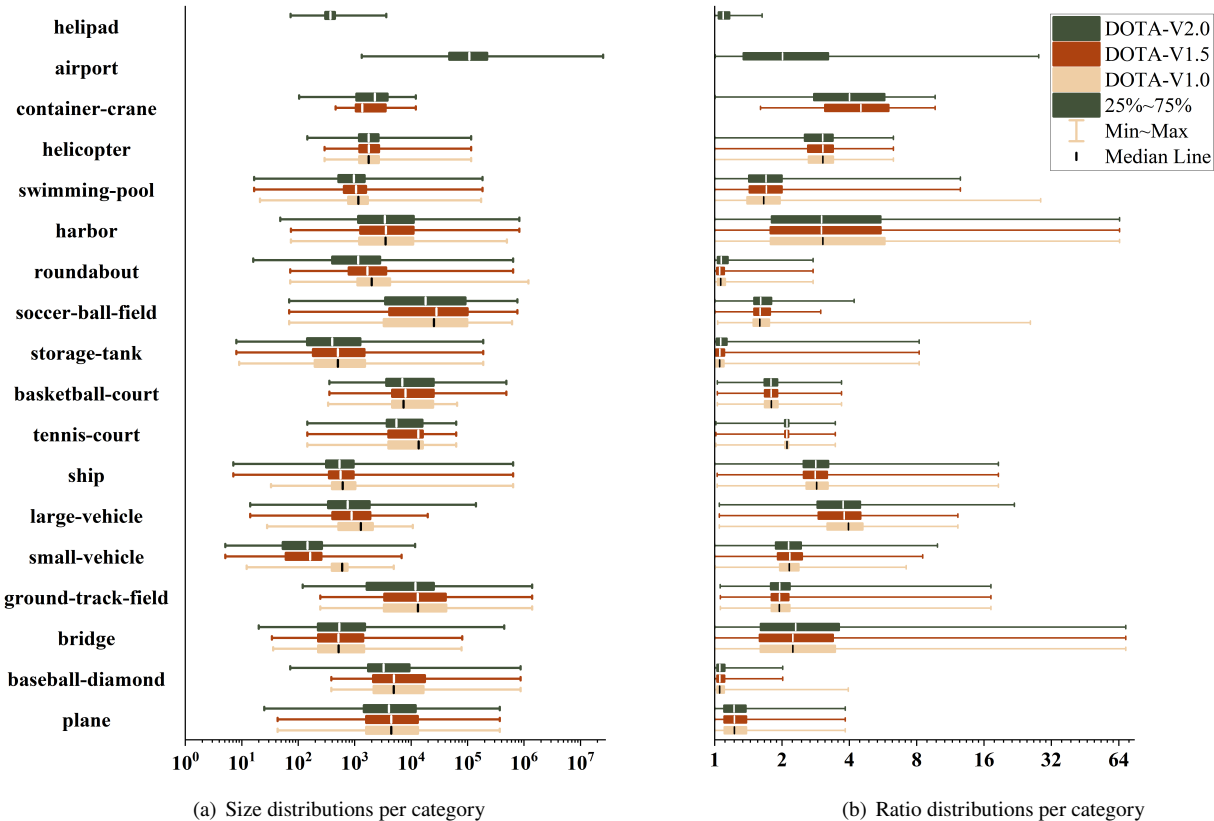


Figure 16: Size and ratio distributions for each category in training and validation subsets of DOTA-V1.0, V1.5, and V2.0 (Xia et al., 2018; Ding et al., 2022)

Figure 16(b) indicates that the aspect ratios of different categories vary greatly. Furthermore, some categories have an extremely large aspect ratio, such as bridge, harbor, and airport. Up to now, DOTA has been the most challenging dataset for oriented object detection, due to its tremendous object instances, large aspect ratio, significant size variance, and complicated aerial scenes. All of these characteristics contribute to DOTA as the de facto benchmark for evaluating the efficacy of oriented object detectors in previous years.